

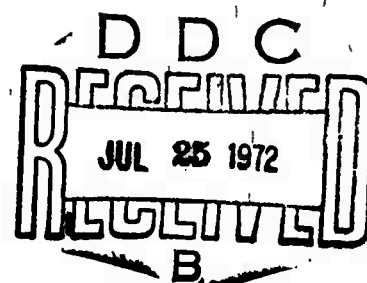
AD 745347

Semi-Annual Progress Report
for the Period January 1, 1972 to May 31, 1972

Glassy Carbons

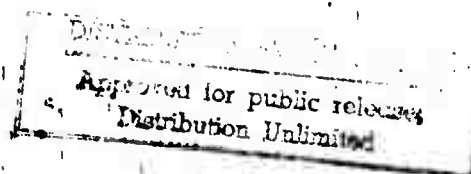
June 1972

Sponsored by
Advanced Research Projects Agency
ARPA Order No. 1824



Department of Materials and Metallurgical Engineering

Reproduced by
NATIONAL TECHNICAL
INFORMATION SERVICE
U S Department of Commerce
Springfield VA 22151



SEE AD
737278

GLASSY CARBONS

Semi-Annual Progress Report for the Period
January 1, 1972 to May 31, 1972

June 1972

Details of Illustrations in
this document may be better
studied on microfiche

ARPA Order Number: 1824
Program Code Number: 1D10
Contractor: The Regents of The University of Michigan
Effective Date of Contract: 1 June 1971
Contract Expiration Date: 31 May 72
Amount of Contract: \$150,263
Contract Number: DAHCl5-71-C-0283
Principle Investigator: Professor Edward E. Huckle
Department of Materials & Metallurgical
Engineering
The University of Michigan
Ann Arbor, Michigan 48104
(313) 764-3302

I

The views and conclusions contained in this document are those of the authors and should not be interpreted as necessarily representing the official policies, either expressed or implied, of the Advanced Research Projects Agency or the U.S. Government.

II

TABLE OF CONTENTS

Summary	iv
I. Introduction	1
II. Materials Preparation	3
III. Structural Studies	5
A. Solid Structure	7
X-Ray Studies	7
Electron Microscopy and Diffraction	26
Thermodynamics	36
B. Pore Structure	40
Electron Scanning Microscopy	41
Helium Pycnometry	41
Surface Area	45
Mercury Porosimetry	45
IV. Property Evaluation	53
Hardness	55
Compressive and Ultimate Tensile Strength	58
Sonic Modulus and Internal Friction	59
Electrical Resistivity	64
References	71

GLASSY CARBONS

Summary

A large group of glassy carbon samples has been produced by controlled curing and pyrolysis of furfural alcohol based resins. Various structural characterizations and key property measurements have also been made.

Crack free samples with apparent densities ranging from .5 to 1.27 gm/cm³, mean pore sizes from 50 Angstroms to 50 microns, B.E.T. surface areas from 20 to 500 m²/gm, elastic modulus from $1.8 \cdot 10^5$ to $7.35 \cdot 10^6$ psi, compressive strength up to 55,000 psi, and tensile strength up to 10,850 psi, have been produced in section thickness up to 1.2 inches.

X-ray and electron diffraction, together with electron microscopy have revealed various structural features at size levels from 20 Angstroms to 200 microns.

GLASSY CARBONS

I. Introduction

This report covers work carried out during the second six month period of the present contract. The major areas of investigation and previous findings were reported in the first semi-annual report¹.

The availability, chemical inertness, and excellent physical and mechanical properties of the disordered carbons form the basis for interest in further understanding the structure of these materials. With an understanding of structural variations possible, further extension in the range of properties achievable can be made. From data previously available in the literature and the early results of this program¹, it has become obvious that "glassy carbon" is not a single material, since even though it contains essentially only carbon atoms, its structure can be varied at all size levels. It seems more appropriate to think of glassy carbon as a material that may have short range atomic coordination with a variable state of crystallinity; but in addition, where rather large amounts of thermally stable voids can be arranged at size levels from 5 Angstroms to 50 microns. As a result, an extremely wide variation in properties can be achieved. The incorporation of voids into materials is not unique. However, it is unique to have up to 30% void remain stable in a material at temperatures

close to sublimation when the pore size is well below 100 Angstroms.

Glassy carbons possess some crystallinity on a scale of the order of 100 Angstroms, but the perfection of the crystallites is very poor by usual standards; and while the crystalline perfection may improve with very high temperature, a well-defined graphitic structure is not achieved without unusual methods. The structure is better described as para-crystalline in analogy to the name invented for polymers. In fact, the glassy carbon structures are best considered polymers with vanishing contents of other than carbon atoms and are certainly related to the polymer structures from which they evolve during controlled pyrolysis. This fact follows since it is possible to vary the structure and properties of a carbon obtained after heating to 3000°C by controlling the thermal history of the polymer in a temperature range below 100°C where polymer structure is being formed. Thus, even though most of the atoms present in the precursor polymer are later removed, the resulting carbon inherits part of the structure.

The present study is largely concerned with studying the structures obtainable together with the simultaneous measurement of certain key physical and mechanical properties. It is desired to achieve in different samples as wide a variation in structure and properties as possible.

The structure is being investigated from the viewpoint of the solid structure and the pore structure. Since significant

differences can be induced in both over a size range of more than four orders of magnitude, no single technique is sufficient. Instead, combined techniques must be used. Each is discussed in detail in the following sections of the report. Representative property measurements are being carried out in conjunction with the structural examinations. In addition to the hardness, strength, and stiffness measurements begun previously, internal friction, and electrical resistivity have been added on a selective basis.

Most of the effort of the present report period has been expended in gathering additional data on the many different sample variations where data were previously lacking.

II. Materials Preparation

During this report period over 550 samples of glassy carbon were prepared with over 100 different processing conditions. The work has continued to concentrate on furfural alcohol and a furfural alcohol resin, Durez 16470* as the carbon yielding material, with para-toluene sulfonic acid (PTSA) as the polymerization catalyst. Catalyst levels from 2 to 20% by weight based on the monomer or resin content have been explored. Temperatures for addition of the catalyst and subsequent curing have been varied from -11°C to 150°C. In all cases where a particularly interesting set of properties have been found, a duplicate set of specimens has been made to check reproducibility. Standard sample cylinders approximately 3 cm in diameter and 20 cm in

*Hooker Chemical Company, North Tonawanda, New York.

length have been adopted. In a few cases, samples up to 4 cm in diameter have also been produced.

The yield of crack free material has continued to improve due mainly to increased care in adding the catalyst to the resin and preventing the trapping of bubbles prior to and during casting. The presence of bubbles has been found to cause cracking in the subsequent pyrolysis of the samples. In most cases, it has been possible to perform a reduced pressure debubbling operation after addition of the catalyst.

In order to yield good material it has been necessary to perform the hardening of the resin systems with a minimum temperature gradient throughout the piece, which often requires cooling after addition of the catalyst. The length of time curing, curing temperature and catalyst level have been varied over wide ranges.

The single most important factor in obtaining crack free materials in pyrolysis is obtaining a uniform slow heating rate. While heating rates have been varied from 5 to 50°C per hour in the range of room temperature to 1000°C, the yield of crack free material is much greater at the slower rates. Rates up to 200°C per hour appear to cause no difficulty in heating material previously pyrolyzed to at least 700°C. Both flowing nitrogen and reduced pressure pyrolysis have been employed. Thus far, flowing nitrogen appears to yield less difficulty with respect to cracking.

On selected samples, carbon recovery and shrinkage data have been gathered. In both cases the data are comparable with

those of the literature, namely a carbon recovery based on the total resin weight of about 55% and linear shrinkage of about 29%.

Inhomogenieties of about 1μ in diameter in the starting resin were noted in the previous report¹. These regions carry through the pyrolysis and cause non-uniformity in the final structure. At present no completely satisfactory method has been found for eliminating this problem.

Rather subtle differences exist in the cured resins which result in different properties after pyrolysis. Thus far no satisfactory means for quantitatively studying the resin have been developed. In the future thermal analysis and possibly infra-red reflection spectroscopy will be investigated as a means of studying the resin systems.

III. Structural Studies

While the eventual goal of this study is to correlate structure at various stages of the process with properties, the results thus far are largely drawn from samples taken at only two processing stages. The first stage corresponds to a maximum temperature exposure in the range 650-1000°C, while the second stage is that formed at about 2000°C. Further exploration of the stages of formation will proceed after appropriate techniques of sample preparation, structural analysis, and property measurement are fully developed.

The techniques chosen for structural examination fall into two broad categories with respect to the information yielded. The first yields (predominantly) information about the state of the solid making up of the structure, while the second deals mainly with the void structure. In the first category this study is employing bright field and dark field transmission electron microscopy, electron diffraction, wide angle X-ray diffraction (pinhole and diffractometer methods) and scanning and electron microscopy. The last two methods also yield information on pore structure.

Additional methods used to establish the pore structure are small angle X-ray scattering, helium pycnometry, mercury porosimetry, and surface adsorption. An attempt is also being made to gain structural information through a precise measurement of the thermodynamics of the equilibrium

$$C_{\text{graphite}} = C_{\text{glassy}}$$

Since the effort required to carry out the above techniques varies substantially, a complete set of data will be collected on only a limited number of samples after screening with more routine tests. Apparent and real (He) density, wide angle X-ray diffraction, scanning electron microscopy (SEM), hardness, compressive strength, tensile strength, and sonic modulus are being run on representative samples of each batch in order to select appropriate samples for more intensive study.

A. Solid Structure

X-Ray Studies

The state of non-graphitizing carbons can be described by the "degree of graphitization" which can be obtained approximately from the measurement of the "crystal sizes" and "interlayer spacing". The measurement of the "crystal size" and the interlayer spacing is being done as a routine on all glassy carbon to obtain an approximate idea of the extent of graphitization. These parameters are obtained from the X-ray profile from the diffractometer. The diameter, L_a , and the height, L_c , of the crystal considered as a right cylinder, are measured in the crystallographic \vec{a} and \vec{c} directions. They can be obtained from the measurement of the broadening of the appropriate X-ray diffraction peaks. The interlayer spacing is obtained from the diffraction angle at which the corresponding peak is found. However, accurate determination of the broadening parameters by a rigorous analysis of the experimental X-ray data is complicated by a number of corrections². The analysis applies strictly to "size" broadening and does not allow for strain effects or for a possible distribution of layer spacings. As a result, the broadening parameters in this report are evaluated directly from the experimental diffractometer traces. However, as pointed out by Short and Walker², even with this so-called crude analysis, the L_c is quite satisfactory. However, the d_{002} is generally higher than obtained by the more rigorous analysis. Nevertheless, the d_{002} and the L_c when obtained without correction are satis-

factory when comparing different glassy-carbons, all run under identical conditions.

Sample Preparation

The glassy carbon samples for the diffractometer study can be either solid discs or powder filled in a cylindrical hole supported at the back by a material having very amorphous structure and low density.

The use of a solid sample gives higher diffracted intensity as it has higher bulk density than the powder. However, the time involved in making a solid disc of uniform thickness is not justified for routine work. Therefore, powder of less than 74μ was used except where noted. The powder was loaded into a sample holder and supported by thin circular papers.

The dimensions of the powder sample are 2.3 cm in diameter and 3.0 cm thickness. The region without any intensity contribution from the brass sample holder is only 2.0 cm in diameter, which is large enough for a diffraction angle (2θ) greater than 18.1° , employing a 1° primary slit. The contribution of paper to the total diffracted intensity is small and negligible.

Scanning Speed and Other Conditions

To obtain an accurate X-ray profile, very slow scanning speed should be employed. However, for the amorphous materials such as glassy carbon $dI/d(2\theta)$ is very small at all (2θ) so that rates up to $\frac{1}{2}^\circ(2\theta)/\text{min.}$ can be used without causing under shoot of the peaks.

Using higher angle slits gives higher intensity with some sacrifice of resolution. In this study a slit of 1° opening was used since this slit allows a scan angle as low as $18.1^\circ(2\theta)$ for the sample diameter of 2.0 cm.

Since low intensity is generally a problem, maximum tube voltage and current are used. Nickel filtered Cu K_α radiation obtained with 45KV and 15ma tube settings was employed throughout.

To obtain accurate portrayal of peak profile, a low value of time constant (4 seconds) was used.

Results

The values of the "crystal size" and the interlayer spacing are given in Table 1 for various glassy carbon samples studied.

The samples have been divided into four types depending upon the appearance of (002) peak. The (002) peak is generally smooth (S) and quite broad. But in some samples appearance of a relatively sharp peak occurs superimposed on the broad 002 reflection. This behavior is designated "2P" since the behavior suggests the presence of two phases. Intermediate cases occur sometimes where the peak becomes "not very smooth" (NVS). In still other samples a sharp peak also is present at the angle expected for well-defined graphite. In this case the peak has been designated "3P". Typical (002) peak shapes are given in the Figures 1 to 5.

The (100) peak of these carbons is not resolved from (101) peak. So strictly speaking, L_a and d_{100} can not be

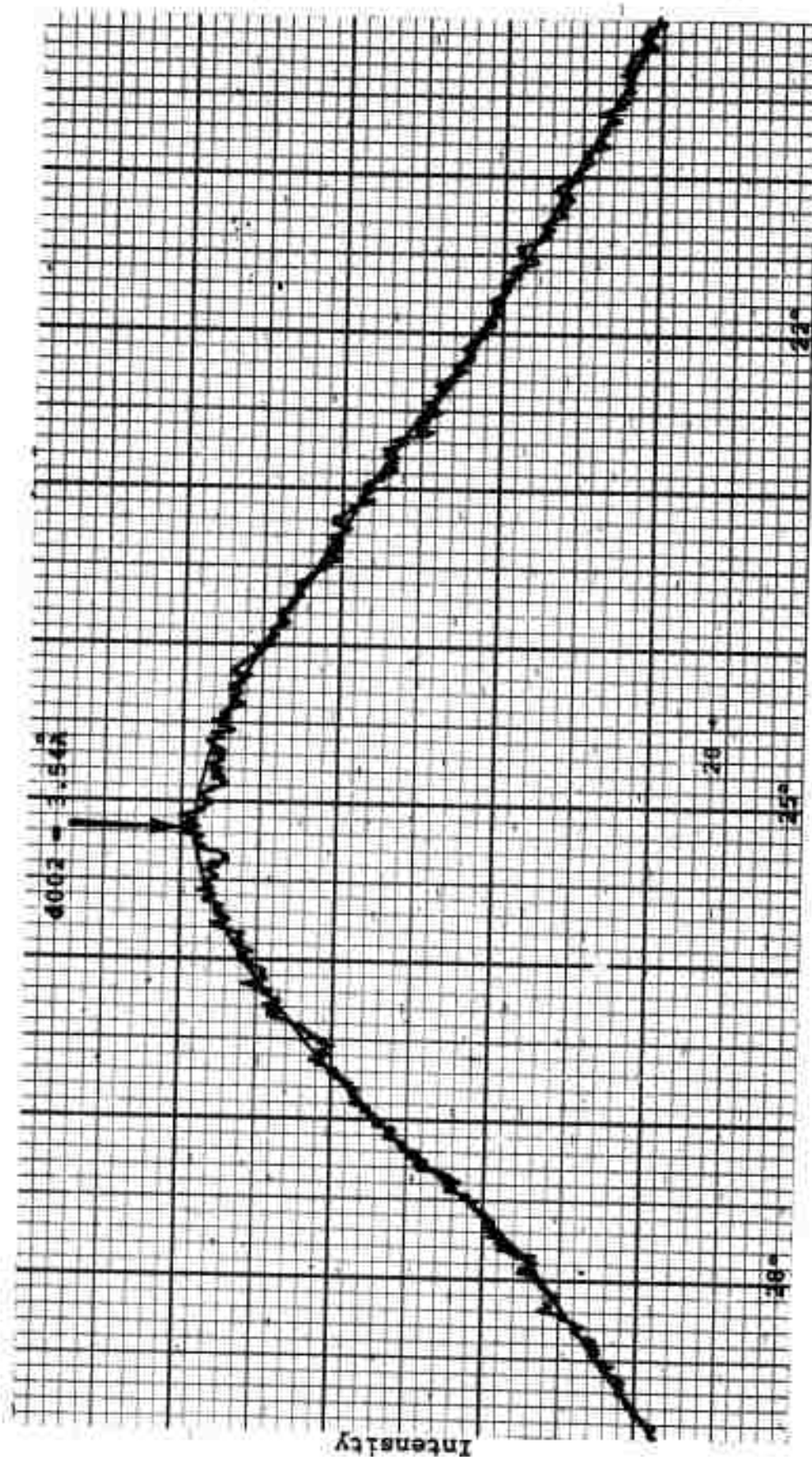


Figure 1. A Typical "S" (002) Peak
317-16, 2000°C

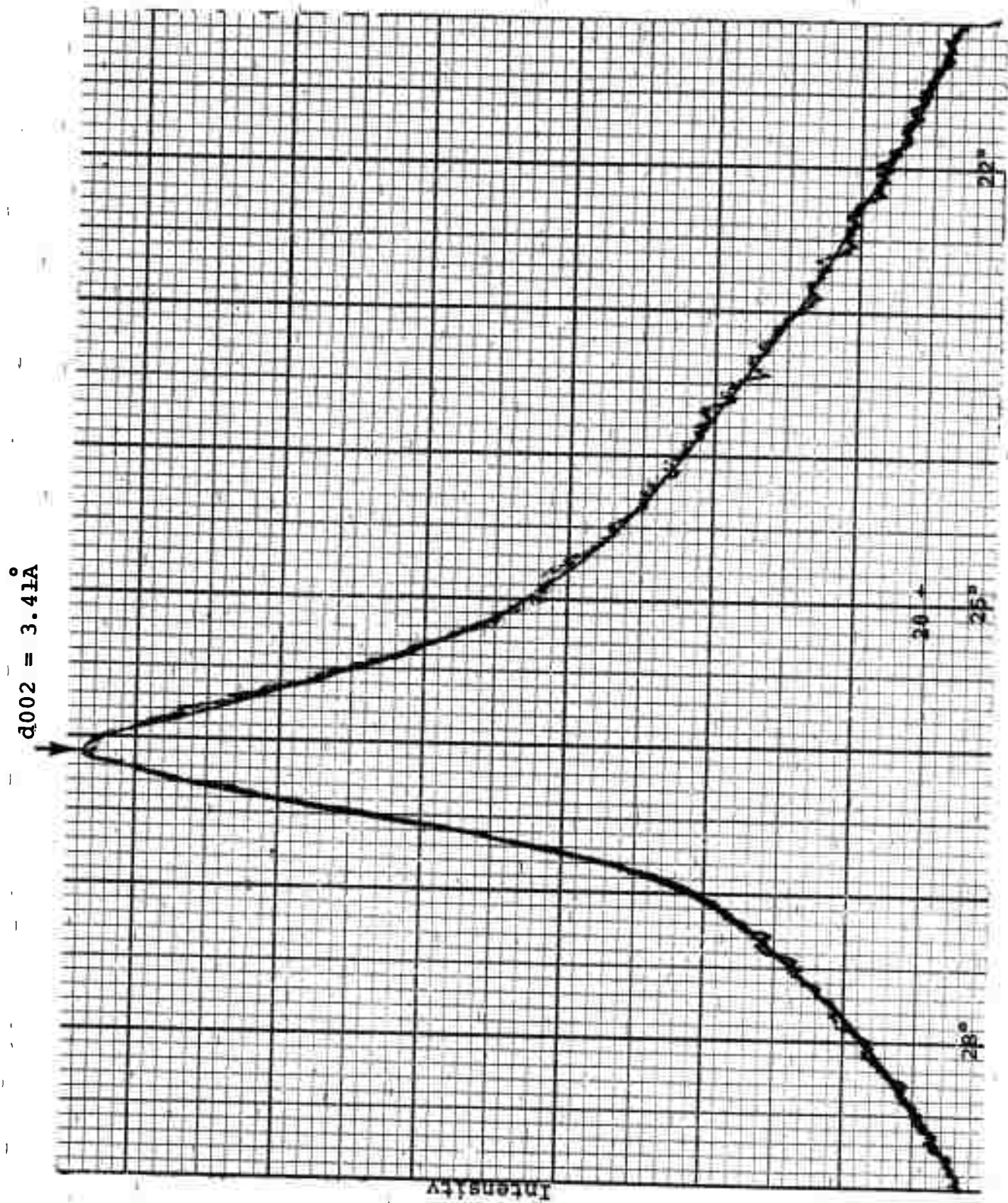


Figure 2. A Typical "s" Peak (002) - highly graphitic sample. 317-33, 2000°C

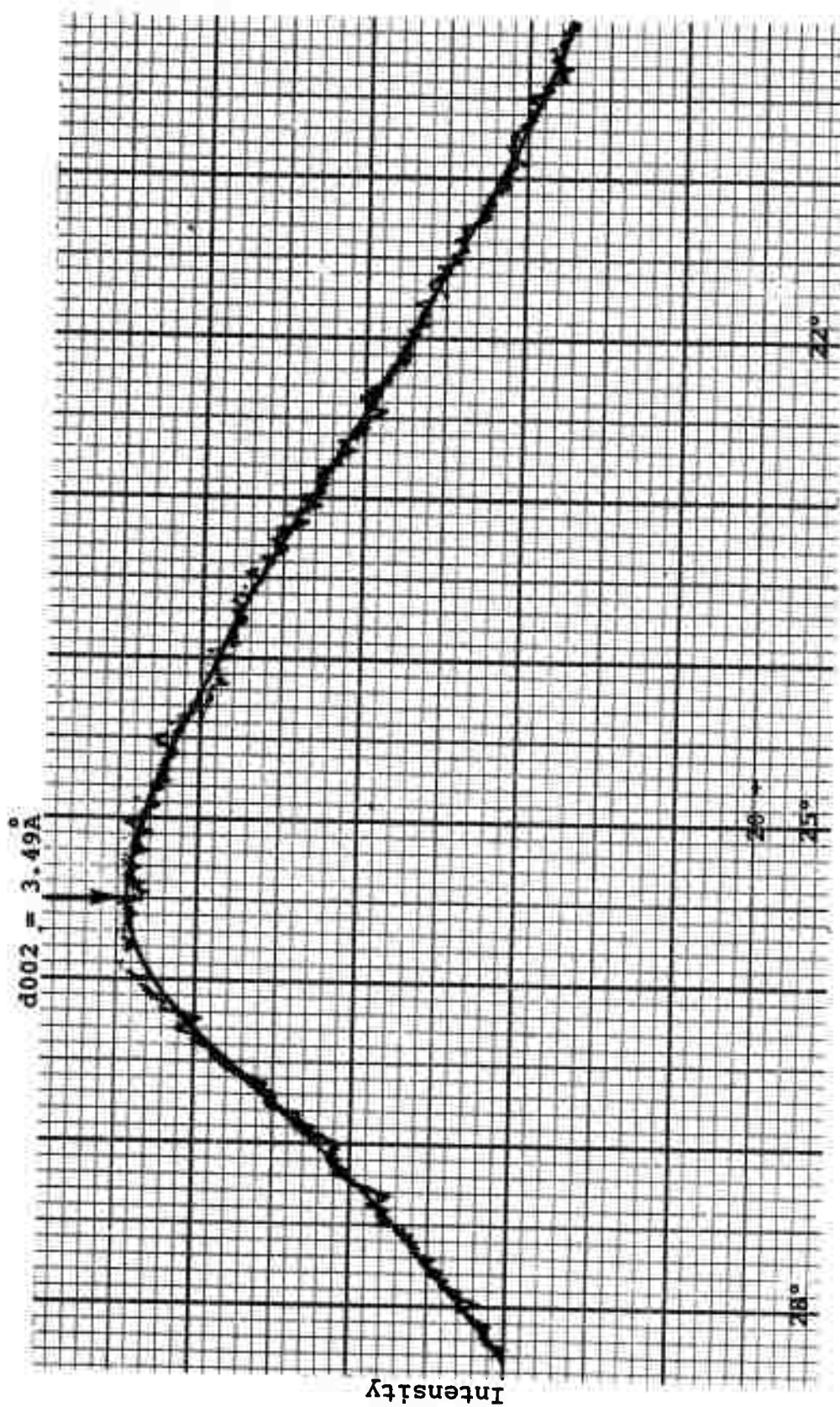


Figure 3. A Typical "NVS" (002) Peak
317-19, 2000°C

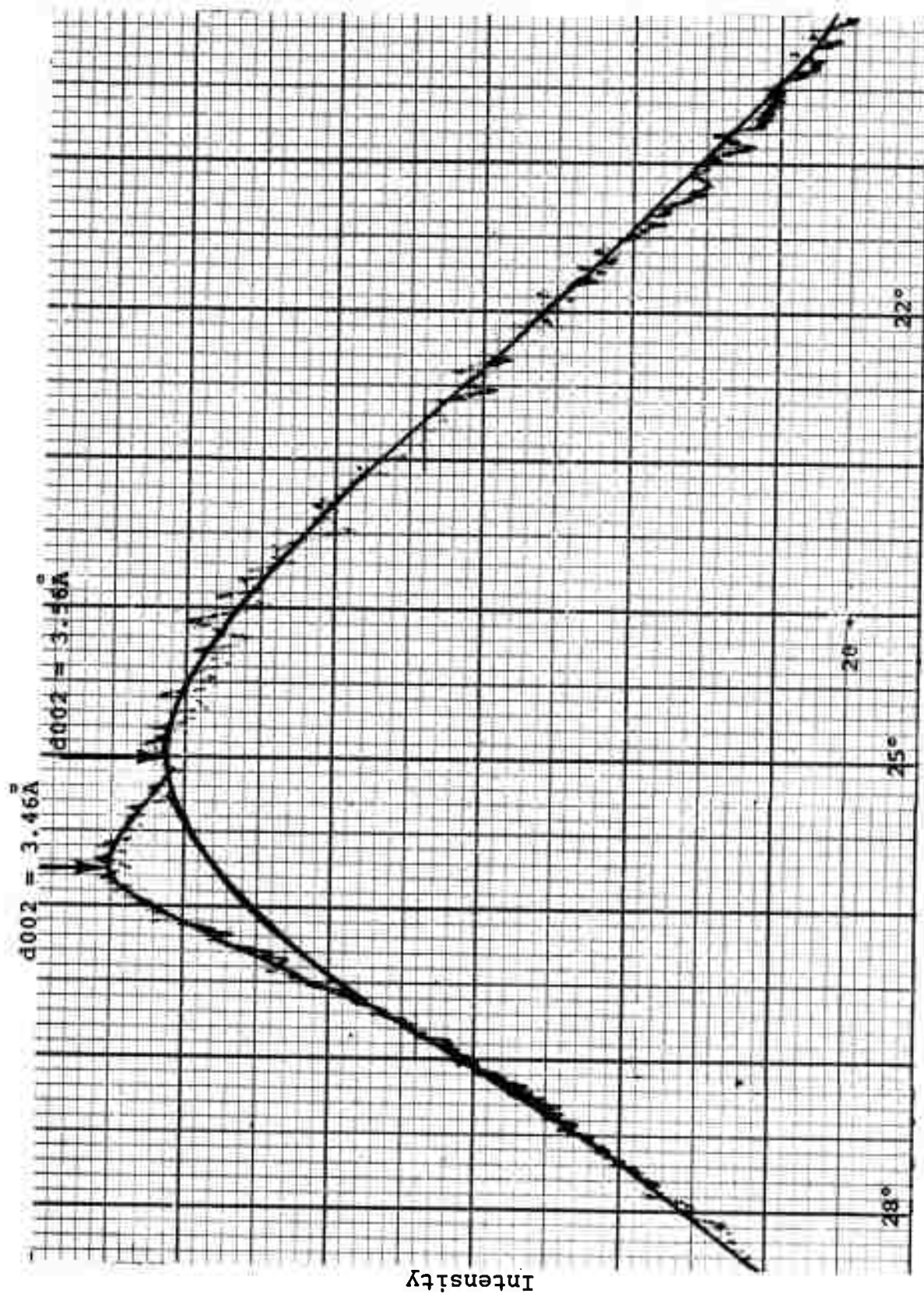


Figure 4. A Typical "2p" (002) Peak
317-8, 2000°C

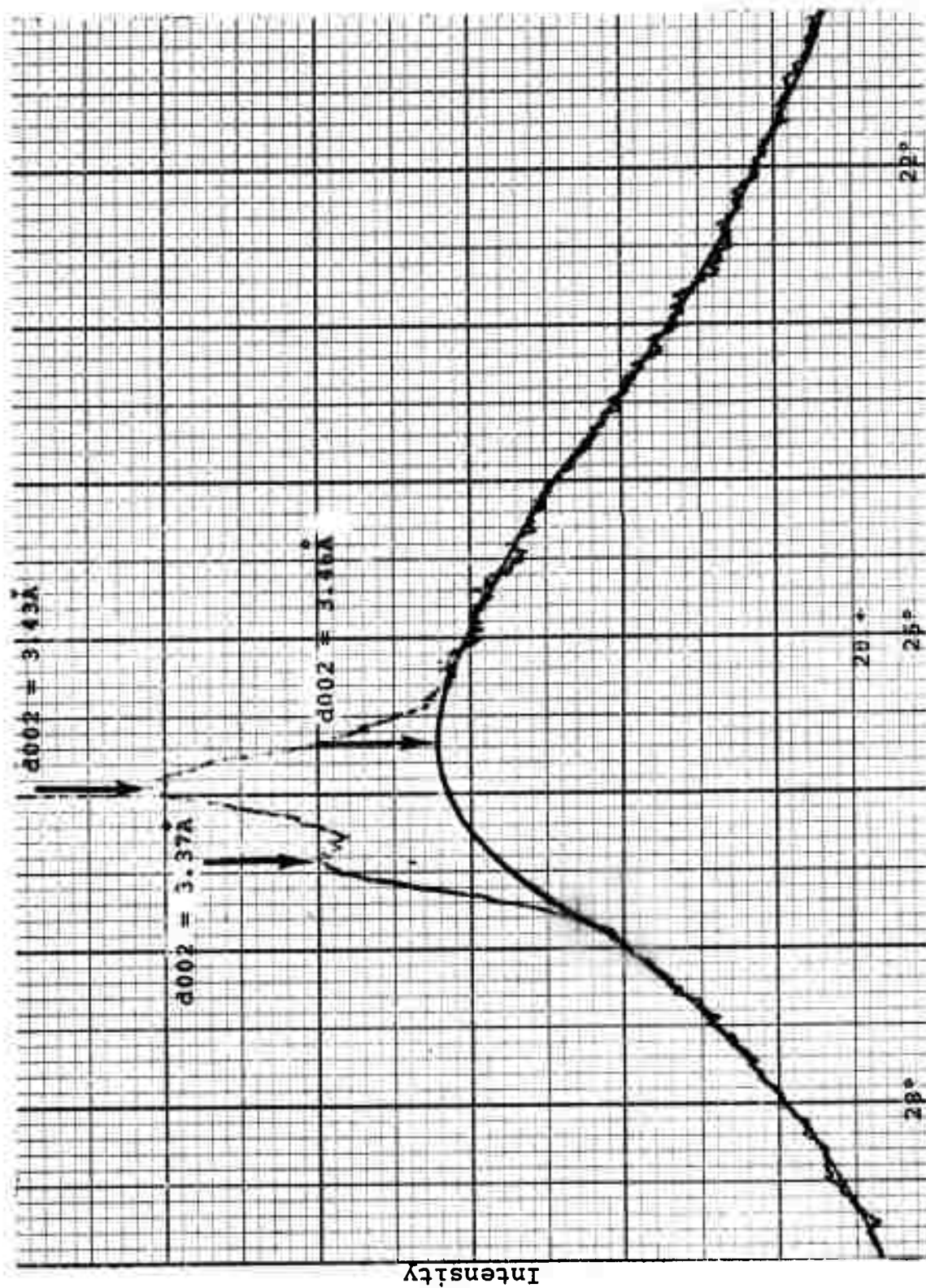


Figure 5. A Typical "3P" (002) Peak
317-48, 2000°C

TABLE 1

SUMMARY OF X-RAY DATA

(All values in Angstroms)

Sample Designation	(002) * Peak Type	d(002)	Lc	d(10)	La
Graphite, solid 3mm & 1mm thick	S	3.37	Very High	2.13	Very High
Graphite	S	3.37	Very High	2.13	Very High
Graphite, natural (Reported)	S	3.35	Very High	2.13	Very High
Graphite, synthetic (Reported)	S	3.37	Very High	2.13	Very High
<u>Commercial Samples</u>					
Lockheed, 2000°C solid, 3mm thick	S	3.53	21.2	2.09	98
Lockheed, 2000°C (Reported)	-	3.56	19	--	--
Beckwith, 2000°C solid, 3mm thick	S	3.55	23.2	2.09	112
Beckwith, 2000°C (Reported)	-	3.54	15	--	50
Tokai, 1000°C solid, 3mm thick	S	3.70	14.2	2.07	43.7
Tokai, 2000°C (Reported)	-	--	--	--	--
Atomergic Chemicals Co. V-25, 2500°C solid, 3mm thick	S	3.52	30.2	2.09	66
Atomergic Chemicals Co. V-25, 2500°C (Reported)	-	--	--	--	--
Atomergic Chemicals Co. V-10, 1000°C	NVS	3.44	45	2.10	70
Atomergic Chemicals Co. V-10, 1000°C (Reported)	-	--	--	--	--

*See symbol list at end of table.

Sample Designation	(002) Peak Type	d (002)	Lc	d (10)	La
311-9, 2000°C	S	3.54	28.0	2.10	57
-19, 700°C	S	3.63	18.0	--	--
-20, 2000°C	S	3.53	27.2	2.10	46
-21, 2000°C	S	3.52	27.2	2.10	54
-22, 2000°C	2P	2.49	29	2.12	>125
		3.45			
-25, 700°C	S	3.70	21.0	--	--
-30A, 2000°C	S	3.51	23.4	2.10	54
-31, 2000°C	S	3.50	25.0	2.10	51
312-8, 2000°C	S	3.52	27.0	2.10	42
-9, 2000°C	2P	3.52	27.0	2.10	57
		3.45			
-10, 700°C	S	3.65	16.2	--	--
-10, 2000°C	S	3.49	35.0	2.11	53
-14, 2000°C	S	3.51	29.0	2.09	61
-14A, 2000°C	3P	3.46	32.0	2.12	>150
		3.43			
		3.36			
-15, 2000°C	S	3.52	27.1	2.11	51
-16, 2000°C	3P	3.47	32.1	2.11	51
		3.43			
		3.36			
-21, 2000°C	S	3.51	30.8	2.10	57
-26, 2000°C	S	3.51	27.8	2.09	48
-28, 2000°C	S	3.51	27.2	2.10	51
-29, 2000°C	S	3.51	34.0	2.10	57
-31, 2000°C, solid 3mm thick	S	3.57	27.6	2.10	56
-32, 2000°C	S	3.51	30.8	2.10	54
-33, 2000°C	NVS	3.48	30.8	2.10	52.8
-34, 2000°C	2P	3.46	33.0	2.11	46.2
		3.44			
-39, 2000°C	S	3.49	29.8	2.10	53
-40, 2000°C	2P	3.48	30.1	2.09	54
		3.45			
-43, 2000°C	2P	3.48	33.2	2.11	51
		3.43			
-44, 2000°C	2P	3.48	42.0	2.11	51
		3.44			
-48, 2000°C	3P	3.46	30.4	2.10	37
		3.43			
		3.37			
-49, 2000°C	S	3.52	31.1	2.11	61
315-1, 2000°C	S	3.53	27.2	2.10	48
-2, 2000°C	2P	3.49	29.0	2.10	54
		3.43			

Sample Designation	(002) Peak Type	d(002)	Lc	d(10)	La
315-3, 700°C	S	3.71	16.2	--	--
-5, 2000°C	2P	3.49	29.0	2.11	54
		3.44			
-8, 2000°C	2P	3.49	28.2	2.10	56
		3.44			
-9, 2000°C	2P	3.47	33	2.11	47
		3.44			
-14, 2000°C	S	3.53	26.3	2.10	54
-18, 2000°C	3P	3.40	45.0	†	†
		3.382			
		3.351			
-20, 680°C	S	3.70	16.3	--	--
-20A, 2000°C	2P	3.53	28.0	2.10	57
		3.43			
-21C, 2000°C	2P	3.52	27.8	2.10	57
		3.43			
-22, 665°C	S	3.67	16.4	--	--
-22, 2000°C	S	3.52	28	2.10	51
-24A, 2000°C	2P	3.47	20	--	--
		3.38			
-25A, 2000°C	S	3.52	26.5	2.09	48
-26B, 2000°C	3P	3.50	26.5	2.10	46
		3.41			
		3.37			
-26C, 680°C	S	3.69	17.1	--	--
-28, 2000°C	2P	3.52	26	2.10	46
		3.43			
-28B, 600°C	S	3.70	16.8	--	--
-30, 2000°C	2P	3.56	24	2.09	48
		3.43			
-31, 680°C	S	3.70	18.2	--	--
-34, 680°C	S	3.69	15.4	--	--
-36, 2000°C	3P	3.52	24.3	2.10	48.5
		3.43			
		3.37			
-45, 2000°C	S	3.49	27.2	2.10	46.6
316-6, 2000°C	NVS	3.50	27.0	2.11	57
-7, 2000°C, Run 1	S	3.49	28.0	2.10	45
-7, 2000°C, Run 2	S	3.52	27.0	2.10	53
-15, 2000°C	2P	3.40	32.0	†	†
-28, 2000°C	S	3.50	27.2	2.10	51
-32, 2000°C	2P	3.42	53.0	†	†
		3.40			

†The position of (10) peak could not be determined due to the presence of MoC and Mo₂C. (104) peak of MoC has d = 2.122 Å, which completely shadows the (10) peak of the samples.

Sample Designation	(002) Peak Type	d(002)	Lc	d(10)	La
317-1, 700°C	S	3.71	20.0	--	--
-1, 2000°C	S	3.46	45.0	2.11	63
-2, 700°C	S	3.68	15.7	--	--
-2, 2000°C	NVS	3.48	24.6	2.09	47
-6, 700°C	S	3.71	13.0	--	--
-6, 2000°C	NVS	3.55	22.0	2.10	55
-7, 700°C	S	3.68	16.0	--	--
-7, 2000°C	NVS	3.46	27.5	2.10	50
-8, 700°C	S	3.71	11.5	--	--
-8, 2000°C	2P	3.56	20.0	2.10	44
		3.46			
-10, 2000°C	NVS	3.48	26.0	2.10	68
-11, 700°C	S	3.71	16.3	--	--
-13, 700°C	S	3.72	15.0	--	--
-13, 2000°C	NVS	3.47	24.0	2.08	66
-14, 700°C	S	3.71	15.7	--	--
-14, 2000°C	NVS	3.45	27.0	2.09	46
-15, 700°C	S	3.71	15.3	--	--
-15, 2000°C	NVS	3.47	26.0	2.09	54
-16, 2000°C	S	3.54	24.0	2.09	53
-18, 2000°C	S	3.59	21.0	2.09	58
-19, 700°C	S	3.68	16.5	--	--
-19, 2000°C	NVS	3.49	30.0	2.09	52
-20, 700°C	S	3.66	17.5	--	--
-20, 2000°C	S	3.50	25.6	2.09	48
-24, 2000°C, Run 1	NVS	3.52	24.0	2.09	45
-24, 2000°C, Run 2	NVS	3.49	21.0	2.09	50
solid, 3mm thick					
-25, 2000°C	S	3.53	20.0	2.09	50
-26, 2000°C, Run 1	NVS	3.48	26.0	2.09	48
-26, 2000°C, Run 2	2P	3.46	24.2	2.10	51
solid, 3mm thick		3.43			
-28, 2000°C	NVS	3.46	25.0	2.09	52
-29, 700°C	2P	3.43	21.5	†	†
		3.42			
-29, 2000°C, Run 1	NVS	3.43	65.0	†	†
-29, 2000°C, Run 2	NVS	3.426	75	†	†
-30, 2000°C	2P	3.44	29.5	†	†
		3.40			
-31A, 2000°C	S	3.58	22.0	2.10	46
-32, 700°C	S				
-32, 2000°C	2P	3.51	23.6	2.08	49
		3.48			

†The position of (10) peak could not be determined due to the presence of MoC and Mo₂C. (104) peak of MoC has d = 2.122 Å, which completely shadows the (10) peak of the samples.

Sample Designation	(002) Peak Type	\bar{a} (002)	Lc	d(10)	La
317-33, 700°C	S	3.68	17.0	--	--
-33, 2000°C	S	3.414	92	2.10	49
-34, 700°C	S	3.68	17.0	--	--
-34, 2000°C	3P	3.44	30.0	2.09	50
		3.42			
		3.36			
-35, 700°C	S	3.71	16.0	--	--
-35, 2000°C	3P	3.50	26.5	2.10	62
		3.43			
		3.36			
-37, 700°C	S	3.68	15.6	--	--
-37, 2000°C	NVS	3.43	43.0	2.10	63
-38, 700°C	S	3.68	15.6	--	--
-38, 2000°C	3P	3.54	25.0	2.09	51
		3.43			
		3.37			
-39, 2000°C, Run 1	3P	3.45	28.0	2.10	52
		3.43			
		3.36			
-39, 2000°C, Run 2 solid, 1mm thick	3P	3.52	24.2	2.09	45
		3.42			
		3.37			
-39, 2000°C, Run 3 solid, 1mm thick	3P	3.52	23.5	2.09	49
		3.41			
		3.37			
-40B, 2000°C	3P	3.49	24.8	2.10	48
		3.42			
		3.36			
-41A, 2000°C	S	3.53	26.5	2.10	48
-41B, 2000°C	S	3.53	28.0	2.10	54
-42, 2000°C	3P	3.49	26.0	2.10	42.6
		3.42			
		3.36			
-43, 2000°C	3P	3.45	26.0	2.09	56
		3.42			
		3.35			
-44, 2000°C	3P	3.48	30.0	2.09	55
		3.42			
		3.36			
-45, 700°C solid, 1mm thick	S	3.75	12.9	--	--
-45, 2000°C, Run 1	3P	3.48	25.0	2.09	60
		3.40			
		3.35			
-45, 2000°C, Run 2	3P	3.46	24.0	2.09	42
		3.42			
		3.35			

Sample Designation	(002) Peak Type	d (002)	Lc	d (10)	La
317-46, 2000°C	3P	3.43 3.42 3.36	31.5	2.10	75
-47, 2000°C	3P	3.50 3.42 3.36	27.0	2.10	60
-48, 700°C, Run 1	S	3.71	16.2	--	--
-48, 700°C, Run 2	S	3.87	17.4	--	--
-48, 2000°C, Run 1	3P	3.45 3.43 3.37	40.0	2.10	60
-48, 2000°C, Run 2 solid, 1mm thick	3P	3.46 3.43 3.37	34.0	2.10	59
-49, 700°C	S	3.71	15.7		
-49, 2000°C, Run 1	3P	3.49 3.41 3.35	29.0	2.09	62
-49, 2000°C, Run 2 solid, 1mm thick	3P	3.46 3.44 3.37	33.0	2.09	60
-50, 700°C	S	3.67	15.6	--	--
318-1, 2000°C	S	3.55	28.0	2.10	54
-2, 2000°C	S	3.51	27.0	2.10	55
-3, 700°C, Run 1	S	3.70	16.7	--	--
-3, 700°C, Run 2	S	3.69	16.7	--	--
-3, 2000°C	2P	3.46 3.41	26.0	2.11	51
-4, 700°C	S	3.66	16.8	--	--
-6A, 2000°C	S	3.50	31.0	2.09	59
-7, 2000°C, Run 1	S	3.50	28.0	2.10	65
-7, 2000°C, Run 2 solid, 3mm thick	S	3.49	28.0	2.10	45
-8, 2000°C, Run 1	S	3.45	39.0	2.10	63
-8, 2000°C, Run 2 solid, 2mm thick	S	3.45	43.5	2.10	77
-9, 2000°C	2P	3.48 3.46	32.5	2.11	57
-10, 520°C	S	3.74	15.2	--	--
-10, 2000°C	S	3.49	33.8	2.12	50
-11, 2000°C, Run 1	NVS	3.42	77	2.10	38
-11, 2000°C, Run 2	NVS	3.43	78	2.11	40
-12, 2000°C	3P	3.49 3.43 3.36	31.4	2.09	59
-13, 2000°C	NVS	3.42	44.0	2.10	58
-14, 700°C	S	3.65	16.0	--	--

Sample Designation	(002) Peak Type	d (002)	Lc	d (10)	La
318-14, 2000°C	3P	3.48 3.43 3.36	30.5	2.10	60
-15, 700°C, Run 1	S	3.75	16.0	--	--
-15, 700°C, Run 2	S	3.75	15.1	--	--
-15, 2000°C	3P	3.45 3.42 3.37	30.2	2.10	60
-16, 700°C	S	3.72	15.7	--	--
-16, 2000°C	2P	3.43 3.41	39.0	2.09	49
-17, 700°C	S	3.68	16.7	--	--
-17, 2000°C	NVS	3.45	42.0	2.11	59
-18, 700°C, Run 1	S	3.68	16.4	--	--
-18, 700°C, Run 2	S	3.71	16.3	--	--
-18, 2000°C	S	3.55	25.6	2.10	44
-19, 2000°C	S	3.52	26.0	2.09	59
-20, 700°C	S	3.67	16.0	--	--
-20, 2000°C	S	3.53	21.0	2.09	48
-21, 700°C, Run 1	S	3.78	14.0	--	--
-21, 700°C, Run 2	S	3.75	15.4	--	--
-21, 2000°C	S	3.55	23.6	2.10	55
-22, 700°C	S	3.70	15.4	--	--
-22, 2000°C, Run 1	NVS	3.44	65	2.10	55
-22, 2000°C, Run 2	NVS	3.44	64	2.11	54
-23, 700°C	S	3.74	16.0	--	--
-23, 2000°C	S	3.63	63	2.10	73
-24, 700°C	S	3.64	16.7	--	--
-24, 2000°C	S	3.44	45	2.10	68
-26, 700°C, Run 1	S	3.69	15.7	--	--
-26, 700°C, Run 2	S	3.75	16.1	--	--
-26, 700°C, Run 3	S	3.69	16.7	--	--
-27, 2000°C	2P	3.45 3.41	35.4	2.10	47
-28, 700°C	S	3.75	18.0	--	--
-28, 2000°C	2P	3.47 3.42	27.0	--	--
-29, 2000°C, Run 1	NVS	3.45	30.0	2.08	62
-29, 2000°C, Run 2	2P	3.50	30.5	2.10	65
solid, 1mm thick		3.44			
-29, 2000°C, Run 3	2P	3.52 3.42	31.0	2.10	60
-30, 700°C	S	3.64	15.2	--	--
-30, 2000°C, Run 1	2P	3.48 3.43	34.1	2.11	69
-30, 2000°C, Run 2	3P	3.45 3.41 3.36	31.0	2.11	63

Sample Designation	(002) Peak Type	d (002)	Lc	d (10)	La
318-31, 2000°C, Run 1	2P	3.45 3.43	35.5	2.10	64
-31, 2000°C, Run 2	3P	3.47 3.41 3.36	31.0	2.11	63
-32, 700°C, Run 1	S	3.64	15.7	--	--
-32, 700°C, Run 2	S	3.63	16.0	--	--
-32, 2000°C	S	3.44	47.0	2.10	65
-33, 700°C	S	3.66	16.7	--	--
-33, 2000°C	NVS	3.46	28	2.11	64
-34, 700°C	S	3.63	16.5	--	--
-34, 2000°C	3P	3.49 3.43 3.36	37.0	2.10	59
-35, 700°C	S	3.71	15.3	--	--
-35, 2000°C	3P	3.50 3.44 3.37	34.0	2.11	67
-36, 700°C	S	3.68	17	--	--
-36, 2000°C	2P	3.51 3.44	28.0	2.10	49
-37, 700°C	S	3.71	16.1	--	--
-37, 2000°C	3P	3.46 3.43 3.376	33.6	2.10	52
-38, 700°C	S	3.71	15.6	--	--
-38, 2000°C	3P	3.47 3.43 3.37	28.0	2.10	49
-39, 700°C, Run 1	S	3.71	17.0	--	--
-39, 700°C, Run 2	S	3.65	17.2	--	--
solid, 1mm thick					
-39, 2000°C	S	3.51	26.1	2.09	60
-40, 700°C	S	3.71	15.0	--	--
-40, 2000°C	2P	3.52 3.45	28.0	2.11	54
-41, 700°C	S	3.71	14.8	--	--
-41, 2000°C	S	3.50	28.0	2.09	57
-43, 700°C, Run 1	S	3.69	17.0	--	--
-43, 700°C, Run 2	S	3.71	13.8	--	--
solid, 1mm thick					
-43, 2000°C	S	3.44	31.0	2.12	58
solid, 3mm thick					
-44, 700°C	S	3.72	15.6	--	--
-44, 2000°C	S	3.55	27.2	2.10	44
-45, 700°C	S	3.71	15.7	--	--
-45, 2000°C	S	3.56	25.4	2.10	46

Sample Designation	(002) Peak Type	d(002)	Lc	d(10)	La
318-46, 700°C	S	3.71	15.9	--	--
-46, 2000°C	S	3.53	26.2	2.11	51
solid, 1mm thick					
-47, 700°C	S	3.71	15.0	--	--
-47, 2000°C	NVS	3.49	29.0	2.10	48
-48, 2000°C, Run 1	S	3.53	26.8	2.10	54
-48, 2000°C, Run 2	S	3.52	29.2	2.10	42
-50, 700°C, Run 1	S	3.71	14.3	--	--
-50, 700°C, Run 2	S	3.71	15.5	--	--
-50, 2000°C	S	3.53	26.0	2.10	46
-51, 2000°C	S	3.50	27.2	2.10	56
-52, 2000°C	S	3.53	26.5	2.10	54
-53, 2000°C, Run 1	S	3.52	26.5	2.10	54
-53, 2000°C, Run 2	S	3.54	30.0	2.10	60
-54, 700°C	S	3.66	17	--	--
-55, 700°C	S	3.71	15.2	--	--
-56, 2000°C	S	3.54	27.0	2.10	54
-58, 700°C	S	3.71	18.0	--	--
-58, 2000°C	NVS	3.51	28.2	2.10	51
-59, 700°C	S	3.68	16.7	--	--
-59, 2000°C	S	3.51	26.0	--	--
-60, 700°C	S	3.70	15.7	--	--
-60, 2000°C	2P	3.47	32	--	--
		3.44			
-61, 700°C	S	3.71	18.6	--	--
-61, 2000°C	S	3.52	23.3	2.09	55
-62, 700°C	S	3.70	15.3	--	--
-62, 2000°C	S	3.56	22.5	2.10	51
321-1, 700°C	S	3.66	5	--	--
-2, 700°C	2P	3.63	17.4	--	--
		3.57			
-2, 2000°C	3P	3.54	22.8	2.10	51.5
		3.43			
		3.38			
-3, 700°C	S	3.64	17.4	--	--
-3, 2000°C	S	3.53	24.3	2.10	51
-4, 700°C	S	3.64	17.2	--	--
-4, 2000°C	-	--	--	--	--
-5, 700°C	S	3.63	15.4	--	--
-5, 2000°C	S	3.49	26.4	2.09	53.7
-6, 700°C	S	3.64	17	--	--
-6, 2000°C	S	3.54	27.7	2.10	48
-7, 700°C	S	3.69	18	--	--
-7, 2000°C	-	--	--	--	--
-8, 700°C	S	3.69	17.5	--	--
-8, 2000°C	-	--	--	--	--

Sample Designation	(002) Peak Type	d (002)	Lc	d (10)	La
321-9, 700°C	S	3.67	17.4	--	--
-9, 2000°C	-	--	--	--	--
-10, 700°C	S	3.67	17.0	--	--
-10, 2000°C	-	--	--	--	--
-11, 700°C	S	3.71	17.0	--	--

Symbols Used in the Tables

(002) Peak Type

- S: "Smooth" (or single phase) Peak
 NVS: "Not Very Smooth" Peak
 2P: "2 Phase" Peak
 3P: "3 Phase" Peak

Experimental Condition

All the samples were run in a Phillips-Norelco Diffractometer using $\text{CuK}\alpha$ radiation under the following conditions:

Tube Voltage: 45KV

Tube Current: 14mA

Proportional Counter Voltage: 1.622 KV

Proportional Counter Time Constant: 4 sec.

Chart Speed: 1/2 inch/min.

Scan Speed: 1/2 degree (2 θ)/min.

Slits: 1°/006"/1° at Primary/Scattering/Secondary

Powder used of thickness of 3mm in all the cases except where otherwise designated.

calculated. However, to get some idea of the size of the crystal in the \vec{a} direction, L_a was calculated from the unresolved (100) and (101) peak which is designated the (10) peak. Therefore, the values of d_{10} and L_a should be interpreted accordingly.

To determine the L_c and L_a a base value of intensity was determined. This base value was taken as the minimum value of intensity in the region between (002) and (10) peak. This minimum value generally occurred near $35-40^\circ$ (2θ). Since in this region the intensity is very small it was determined by manual rotation of the goniometer. A line parallel to the base line was drawn at $3/4$ of the peak height above the base line. Then use of the Scherrer's equation,

$$L = \frac{0.51\lambda}{\Delta(\sin\theta)}$$

yielded the required value of crystal size.

In the cases of "2P" or "3P", a smooth curve was drawn through the profile. The " L_c " reported are for the smoothed broad peak. The other value of d_{002} given is lower than d_{002} corresponding to the broad peak.

Discussion

Use of powder in place of the solid sample was justified as there was excellent agreement within experimental errors between values obtained by both ways. For example 317-29 (2000°C), 317-39 (2000°C), 317-45 (2000°C), 317-48 (2000°C), 317-49 (2000°C), 318-8 (2000°C), etc., show good agreement. Thus use of powder is made and has a distinct advantage over solid samples as the

sample can be made very uniform while minimizing sample preparation time.

In general, the d_{002} and L_c data for the broad "S" type patterns is similar to that reported in the literature. Representative reported values together with experimental determinations on various commercial glassy carbons and graphites are reported in Table 1.

Correlation of the X-ray parameters with other properties is underway. However, no definite conclusions can be drawn at the present time.

Electron Microscopy and Diffraction

Transmission electron microscopy (TEM) was used to examine the microstructure of selected glassy carbon samples. With a resolving power of 20 Angstroms, bright and dark field (TEM) was capable of viewing particles or structural features the size of the "crystallites" suggested by X-ray line broadening analysis. TEM was therefore used as a tool to study the material's micro-homogeneity and the structure on a size scale down to 20 Angstroms. With the capabilities of selected area electron diffraction, the variation of d_{002} and d_{10} within a sample was also studied and compared to the average d-spacing obtained with X-ray diffraction.

As reported earlier¹, the most successful TEM results were obtained by viewing small particles of the sample directly. These particles (0.1-1.0 μ in diameter), obtained by filing,

were deposited on a 400 mesh copper microscope grid. The particles adhered to the grid bars, thereby exposing edges thin enough for transmission of the electron beam. A number of samples prepared under different processing conditions were analyzed.

Bright field electron micrographs, obtained at magnifications of 36,400 and 66,300X revealed similar structural features to those reported previously¹. In general, irregularly shaped platelets 150-500 \AA in diameter, which contained a granular texture 20-70 \AA in diameter, were observed. The granular texture, in agreement with the previous findings, was more distinct in samples baked at 2000°C than in those baked at 700°C. The characteristic platelet and granular diameters are listed in Table 2.

At the present time it is difficult to draw a conclusion relating platelet size to processing and properties due to the large variation in platelet sizes and regularity. More samples must be studied in detail.

The granular texture size recorded in Table 2 is shown to be comparable to the crystallite size, L_a , as measured by X-ray line broadening. This suggests that the granular texture represents small para-crystalline regions. In support of this suggestion is the observation that a well-defined texture is not observed in the 700°C samples since X-ray line broadening gives values for L_c of less than 20 \AA , which is below the minimum resolution of the microscope. This suggests that the glassy carbon materials crystallize by the formation of small "crystallites" and that the perfection of these crystallites improves with in-

TABLE 2

Sizes of the structural features observed in bright and dark field electron micrographs are compared to crystallite sizes obtained from X-ray analysis.

Sample #	Platelet	Granulation*	Dark	X-Ray (\AA)	
	Dia. \AA	Dia. \AA	Field (\AA)**	Lc	La
311-19, 2000°C	150-500	30-40	20-40	--	--
311-19, 750°C ^x	150-350	20-30	No diffr. areas	14	19
312-31, 2000°C	200-500	20-45	20-45	27.6	56
317-24, 2000°C	250	42	60 [†]	24	45
317-29, 2000°C	>250	60	30-70 [†]	65-75	--
317-45, 2000°C	>500	30	--	25	60
318-22, 2000°C	>500	40-60	35	65	55
318-22, 700°C	250	Ill-defined	None	15.7	
318-23, 2000°C	250	50	50	63	73
318-23, 700°C	Ill-defined	--	None	16	--
318-29, 2000°C ^x	>500	30-40	60	31	63

*Diameter corresponds to distances between nearest neighbors.

**Diameter of diffracting regions obtained from 002 halo.

[†]Dark field from 002 spots reveal diffracting regions of sizes up to 500 \AA in diameter.

^xA second structural feature was observed in the bright field micrographs of these samples. This new feature appeared to be long regular cylinders 500 \AA in diameter by about 1 μ long. Regular striations along the length were spaced 45 \AA apart. (See Figure 7).

creasing temperatures.

Occasionally, platelets in the 2000°C samples did not show the granulated textures but were relatively smooth as shown in Figure 6 for sample 318-22, 2000°C. This smooth surface appears similar to the platelets found in 700°C samples, suggesting that the sample is inhomogeneous on a microscale. Another exceptional feature was observed, but only in samples 318-29, 2000°C and 311-19, 750°C. Instead of irregular platelets, the features observed were cylindrical in shape, with a size of 500Å diameter by about 1μ long, and contained regular 45Å wide striations along the cylinder axis. The striations appear to consist of a granular texture as shown in Figure 7, which suggests that possible further crystallization occurs by the alignment of the previously discussed granules as has been observed in polymer crystallization.

Dark field electron micrographs, obtained from the 002 reflection, reveal as bright spots regions or "crystallites" of specific orientations. The objective apperture was placed either over a portion of the 002 Debye-Scherrer ring (See Figure 8-b, circle c) or over an 002 spot reflection (see Figure 8-b, circle d). Examples of typical dark field micrographs are shown in Figure 8-c,d for sample 317-29, 2000°C. The dark field from the 002 ring shows bright spots indicating diffraction regions 30-70Å in diameter (Figure 8-c), whereas the dark field from an 002 spot shows additional larger diffracting regions, in some cases 500Å in diameter (Figure 8-d). This suggests that the "spots" in the diffraction pattern are from exceptionally large crystallites.

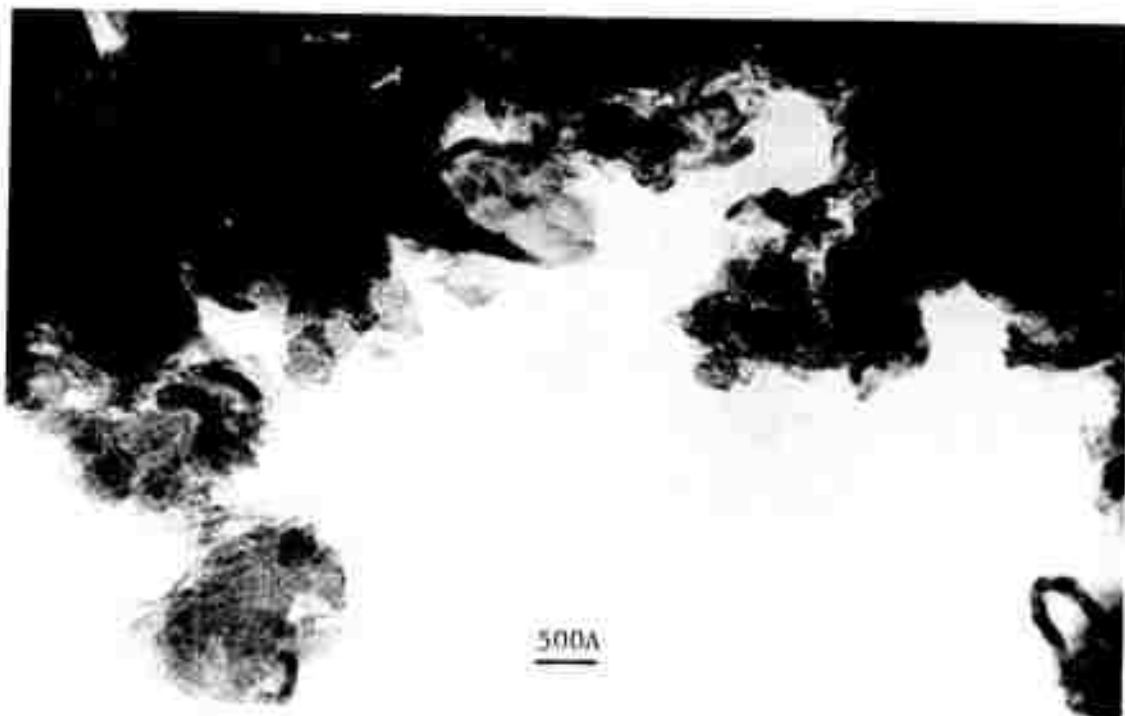


Figure 6. Sample 318-22, 2000°C. Typical platelet and granular features are shown in addition to an exceptionally smooth platelet feature which is occasionally observed.

Reproduced from
best available copy.

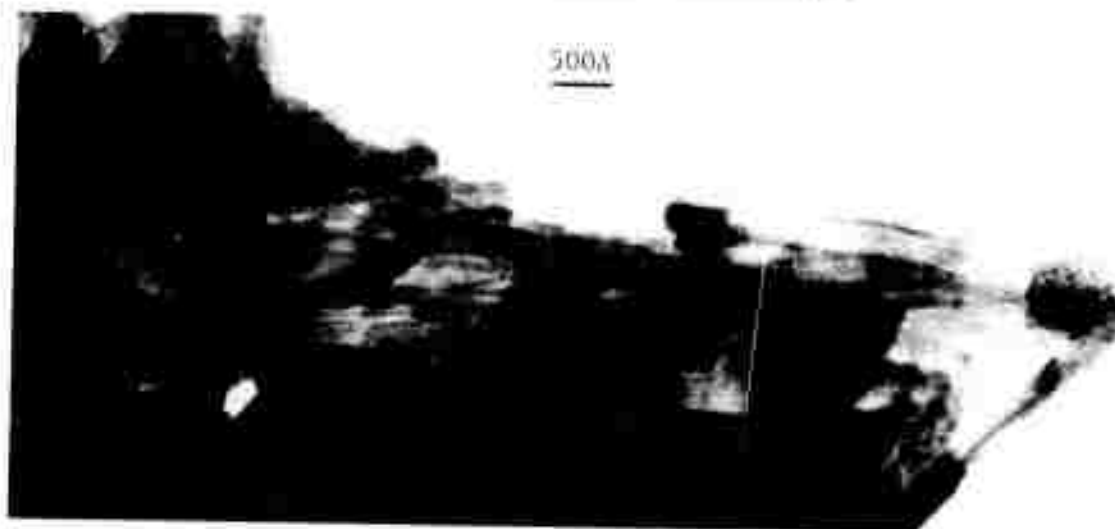


Figure 7. Cylindrical-type features observed only in samples 318-29, 2000°C and 311-19, 750°C. This is an exceptional case even within these samples.

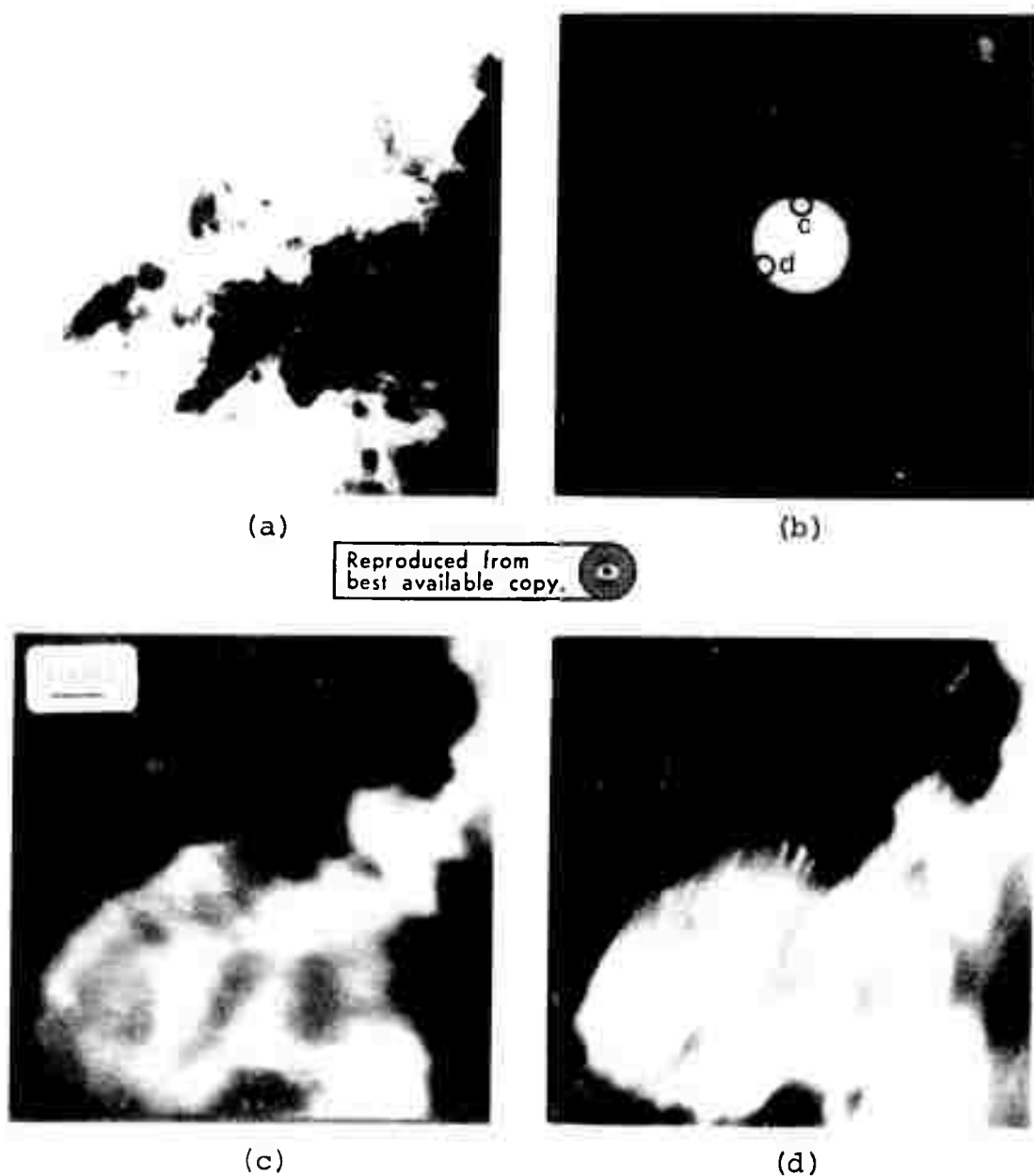


Figure 8. Sample 317-29, 2000°C. (a) Bright field electron micrograph. (b) Selected area electron diffraction pattern showing 002 ring, 002 spots and 10 ring. The 110 ring did not reproduce. Circles c and d show the aperture size and location used for the dark field micrographs c and d, respectively. (c) Dark field micrograph from 002 ring. (d) Dark field micrograph from 002 spot.

In general, the dark field diffracting regions from the 002 rings show particles similar in size to the granulation found in the bright field and in agreement with X-ray analysis. (See Table 2.) This suggests that the granular texture observed in the bright field is a crystalline texture, since the dark field micrographs were obtained from crystalline reflections. A comparison between the two dark field images from the same specimen, but from different regions of the 002 ring, shows different diffracting regions. This implies that the "bright spots" are not due to differences in density or thickness but are from crystalline reflections of specific orientations.

Dark field micrographs could not be obtained for the 700°C samples since the 002 ring was extremely diffuse and often times not even detectable. In addition, dark field micrographs using the 10 ring did not show any diffracting regions possibly because of the low intensity of this ring.

Selected area electron diffraction patterns in most cases displayed three diffuse Debye-Scherrer rings corresponding to the (110), (10) and (002) planes (See Figure 8-b). The sharpness of these rings varied from sample to sample and from area to area within a particular sample, but in general were sharper for the 2000°C samples. This suggests either the sample contains "crystals" having an imperfect lattice and/or contains many small crystals. In addition, it shows that a particular sample is not homogeneous.

In addition to Debye rings, some of the diffraction patterns (more prevalent in the 2000°C samples) contained diffrac-

tion spots (See Figure 8-b). The spots often were superimposed on the Debye rings and in some cases were slightly displaced from the ring showing a smaller d-spacing. The presence of diffraction spots suggests that larger and/or more perfect crystals are present in that particular area.

There was, in general, good agreement between the d-spacings of the (hko) reflections of graphite and the glassy carbon samples as shown in Table 3. However, for (hkl) reflections ($l \neq 0$) the glassy carbon samples always showed a larger d-spacing than that found for graphite, although some diffracting spots tended to approach the graphite values. The d_{002} spacings were in general smaller or closer to the graphite values for the 2000°C samples. This substantiates the well-known tendency toward graphitization with higher pyrolysis temperature. In addition the d_{002} spacings varied from sample to sample and from area to area showing that the samples are not completely homogeneous on a microscale, but vary in packing efficiency. However, Table 4 shows that the average d_{002} spacings from electron diffraction agrees favorably with the values obtained from X-ray.

Often additional diffracting maxima were observed. Table 3 shows that second order reflections (004) and (200) were observed for a number of samples although these samples were not necessarily the samples showing the closest agreement with graphite. The detection of these peaks may be due just to longer exposure of the diffraction pattern and may not indicate greater perfection. One diffraction pattern for sample 317-29, 2000°C

TABLE 3

Selected Area Electron Diffraction Results

Sample #	002	Index							
		100	101	102	004	103	110	112	006
Graphite** 311-19, 2000°C 311-19, 700°C	3.35	2.13	2.04	1.801	1.675	1.541	1.230	1.154	1.117
	3.45	2.09							200
	None†	2.54					1.24		
312-31, 2000°C 317-24, 2000°C	3.52*	2.15					1.32		1.07
	3.53	2.12			1.74		1.24		
	3.53s	2.16			1.77		1.27		1.07
	3.67s	2.16					1.23		
317-29, 2000°C	3.53								
	3.5	2.12					1.23		
	3.42	2.12					1.23		
	3.47	2.12					1.23		
	3.5	2.11	2.09s	1.99s	1.71s		1.24s		1.06
317-45, 2000°C 318-22, 2000°C 318-22, 700°C	3.35s								
	3.5s	2.1			1.75s		1.23		1.06
	3.5	2.1					1.23	1.17	
	3.37s	2.07					1.21s		
318-23, 2000°C 318-23, 700°C 318-29, 2000°C	3.5	2.1					1.23		
	3.42s	2.11			1.74		1.23		
	3.5s	2.10			1.74		1.23		
	None	2.07					1.23		1.07
	3.45†	2.12			1.72	1.54	1.32		1.07
		2.6					1.28		

†From "cylindrical-type" structure.

*Exceptional case (first set of values is most common).

**Kikheev (1957) [$A_c = 2.462\text{\AA}$, $C = 6.701\text{\AA}$]

In addition to Debye-Scherrer rings, a number of sharp diffracting spots were observed on or close to the ring.

TABLE 4

Electron diffraction results are compared to X-ray diffraction results for d002 and d10 spacings (Å).

<u>Sample #</u>	<u>X-Ray</u>		<u>Electron Diffraction</u>		<u>Density (g/cc)</u>
	<u>d002</u>	<u>d10</u>	<u>d002</u>	<u>d10</u>	
Graphite	3.35	2.13			
311-19, 2000°C	3.56	2.17	3.45	2.09	
311-19, 750°C	3.7	2.19	None	2.07	1.17
312-31, 2000°C	3.54	2.12	3.53	2.16	1.41
317-24, 2000°C	3.50	2.1	3.53 ^S	2.10 ^S	1.57
317-29, 2000°C	3.43	--	3.35 ^S	2.12	1.46
			3.45		
317-45, 2000°C	3.35	2.09	3.5	2.1	
	3.48				
318-22, 2000°C	3.44	2.10	3.37 ^S	2.07	
318-22, 700°C	3.7	--	3.5	2.11	
			3.42 ^S		
318-23, 2000°C	3.43	2.1	3.5 ^S	2.1	
318-23, 700°C	3.74	--	None	2.07	
318-29, 2000°C*	3.45	2.08	3.45	2.12	

^SIn addition to Debye-Scherrer rings, a number of sharp diffracting spots were observed on or close to the ring.

*Numerous reflections were observed, see Table 3.

showed (101) and (102) reflections. This was an area showing $d_{002} = 3.35\text{\AA}$, the same as graphite. This suggests that these extra reflections are due to the increased crystalline perfection in this area of the sample.

The "cylindrical-type" structures found in samples 311-19, 700°C and 318-29, 2000°C did not show a (002) reflection although they did show a (100), (200) and (110) reflection (See Table 3). In addition they exhibited a d-spacing of 2.54-2.60 \AA which could not be indexed.

In summary, it appears that the "granulated structure" observed in bright field is the crystallite structure observed in dark field and X-ray line broadening. The samples are not homogeneous with d_{002} -spacings varying within one sample from 3.35 to 3.5 \AA for example, although d_{10} varies only between 2.10 and 2.12 \AA in the same sample. Occasionally, "cylindrical" or "smooth" structures are observed in contrast to the "platelet-granular" structure. More extensive work will have to be carried out in order to relate these findings to preparation variables and to physical properties, although it can be concluded that higher baking temperatures tend to graphitize the glassy carbon material.

Thermodynamics

Although there are diverse methods for gaining information about the structure of solids on various size scales, each has its drawbacks in sensitivity, interpretation, and in ease of measurement when applied to carbon which is not well crystallized.

As a result a thermodynamic method has been proposed³.

Since the reaction

$$C_{\text{graphite}} = C_{\text{glassy}}$$

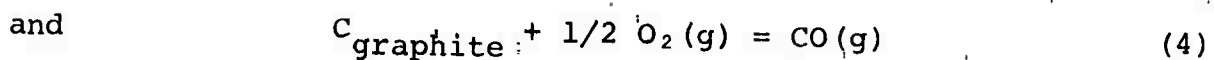
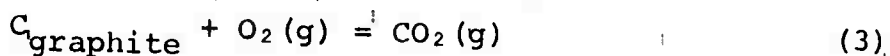
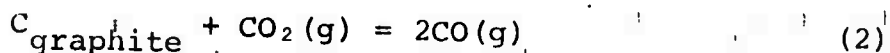
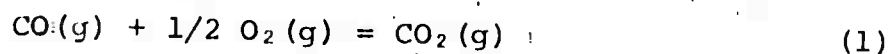
involves no change in composition, the enthalpy (ΔH) and entropy (ΔS) represent a two parameter measure of the structural difference of a glassy carbon relative to graphite.

An accurate determination of the Gibbs free energy for the reaction over a range in temperature allows the separate evaluation of both ΔH and ΔS . The specific heat for crystalline graphite has been measured and at least one study of specific heat of glassy carbon has been made. With the specific heat data for graphite and glassy carbon, a separation of both the enthalpy and entropy into vibrational and configuration components can be made. This procedure thus yields a four parameter measure of the average difference between a given glassy carbon structure and that of graphite. The purely configurational enthalpy and entropy have a very straight-forward meaning as numerical measures of the difference in bonding energy due to disordering, and the degree of disordering respectively. Differences in the vibrational parts result from the effect of differences in average bond strength on the atomic vibrations which determine the specific heat.

In principle it is possible to calculate the configurational entropy for various simple structural models and compare for consistency with the measured value. This procedure can

rule out some models, but never establish the existence of a given model. However, whatever the real structure, the data becomes a numerical measure of the disorder relative to graphite of a given carbon.

In order to be successful, the above plan must be capable of measuring ΔG as a function of temperature with high precision. Electrochemical cells using solid oxide electrolytes, as well as fused salt cells appear to offer the possibility of such a measurement³. These measurements should not be influenced by minor impurities and also will yield as a by-product more accurate and direct data on the equilibria



In spite of the importance of these reactions, such direct free energy measurements have not been carried out. All of the presently available thermodynamic information on carbon-oxygen equilibria is based solely on calorimetry combined with statistically calculated entropies for the gases. The accuracy of the above data depends on the ash content and crystallinity of the graphite and should be determined by direct measurement.

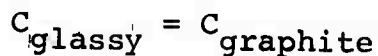
A system of calibration runs has been carried out in order to insure the reliability of the experimental cells. In addition to the experimental confirmation presented previously¹

for reaction (1) and the free energies of formation for NiO, CoO, and FeO, an excellent confirmation has been now obtained for the reaction



A stable cell operation was only obtainable above 950°C. The oxygen pressure for this cell is quite close to that contemplated in the various carbon-oxygen reactions.

In addition a few preliminary runs have been completed for the reaction:

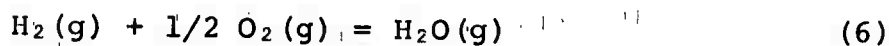


using the fused salt cell;

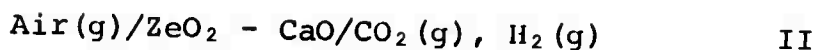
Glassy Carbon/CaC₂ in CaCl₂/Graphite

The emf was high enough (about 20 mv) to be measured accurately and appeared to be quite stable. Graphite was found, as expected, to have the lower free energy at all temperatures studied (800-1000°C). Minor modifications of the experimental apparatus are now being completed prior to precision runs.

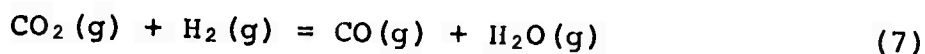
An additional cell has been proposed and evaluated as a means of obtaining the thermodynamic properties of either reaction (1) or



The cell



has been run for several conditions. If an initial mixture of $\text{CO}_2(\text{g})$ and $\text{H}_2(\text{g})$ is allowed to react according to



the following expression can be derived for the equilibrium constant of reaction (1).

$$K_I = \left(\frac{P_{\text{CO}_2}}{P_{\text{H}_2}} \right)_{\text{Initial}} \left(P_{\text{O}_2}^{-1/2} e^{2EF/RT} + \frac{1}{K_{II}} P_{\text{O}_2}^{-1} e^{4EF/RT} \right) - P_{\text{O}_2}^{-1/2} e^{2EF/RT}$$

where P_{O_2} is the oxygen partial pressure at the left electrode in cell II, E is the reversible emf, F is Faraday's constant, R is gas constant, T is absolute temperature, and K_{II} is the equilibrium constant of reaction (6).

Using this method the agreement of the data thus far obtained with published results is within 2%.

B. Pore Structure

The details of the pore structure are being investigated with a variety of techniques. Thus far no useful results have been obtained with small angle X-ray scattering due to a problem with interfacing the diffraction equipment with the counting electronics. After resolution of this problem, this technique will be employed on a limited number of samples to measure size

of pore structure in the range 20-100 \AA .

Electron Scanning Microscopy

Electron scanning microscopy is employed on a fracture surface of each sample to obtain additional information on the pore structure. For the coarser materials ($>200\text{\AA}$) the pore structure is easily discernible with this method. However, for the finer materials, the size of the pores is equal to or finer than the 100 \AA resolving power of the instrument, rendering the determination of quantitative information impossible. Also the SEM pictures show a surface roughness of the same order of size as the pore structure which makes pore size assessment difficult.

At present results are available for approximately 60 samples representing various processing conditions. Unfortunately, most of the samples examined have not yet been subject to Hg-porosimetry for comparative purposes.

Examples of the typical structures observed are shown in Figures 9 and 10. From Figure 9 it can be seen that there is no major change in pore size between 700°C and the 2000°C samples. A sample with a much finer pore structure is shown in Figure 10. Figure 11 shows examples of two samples with a relatively coarse pore structure and the presence of a large agglomerate believed to originate from particles in the original resin.

Helium Pycnometry

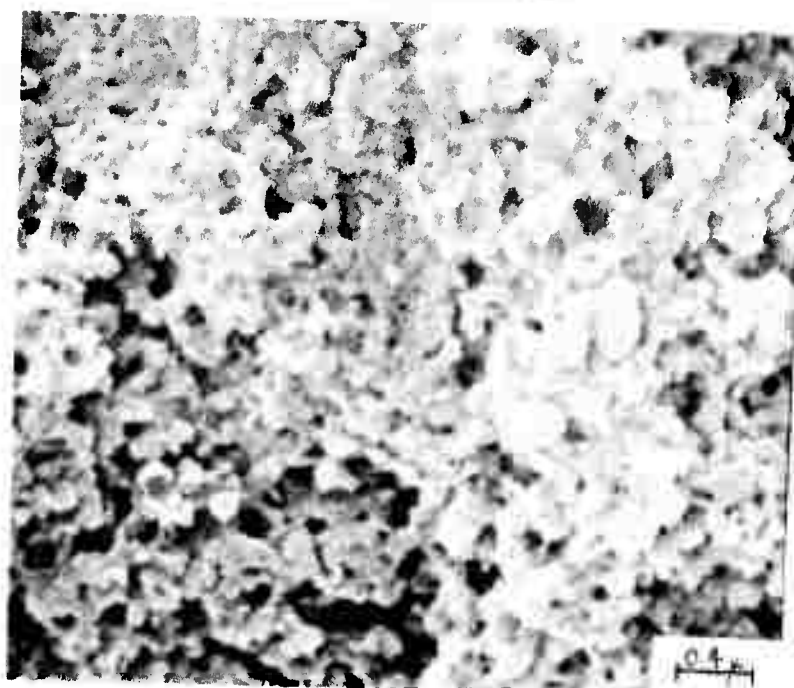
As a routine characterization of the pore volume open to He, the real density is being measured in a commercial



Sample 317-14, 700°C

25,000X

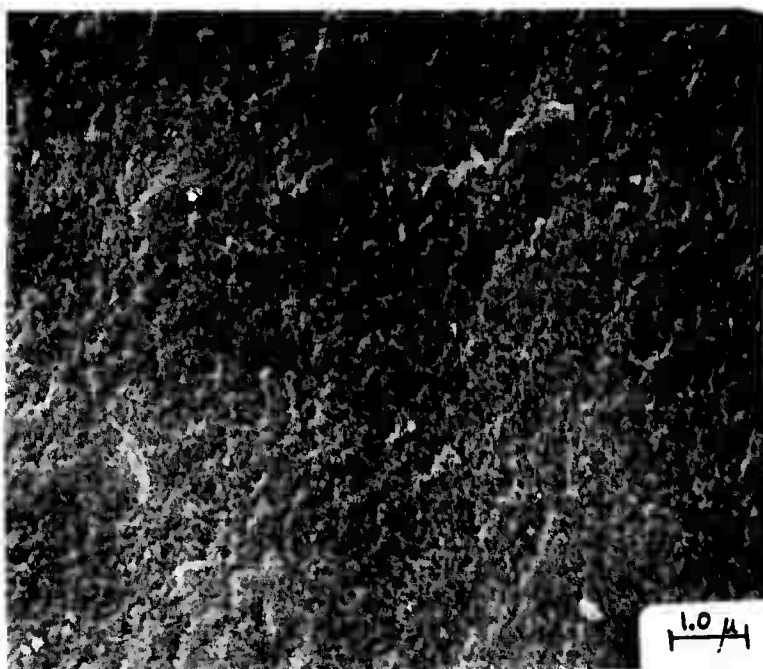
Reproduced from
best available copy.



Sample 317-14, 2000°C

25,000X

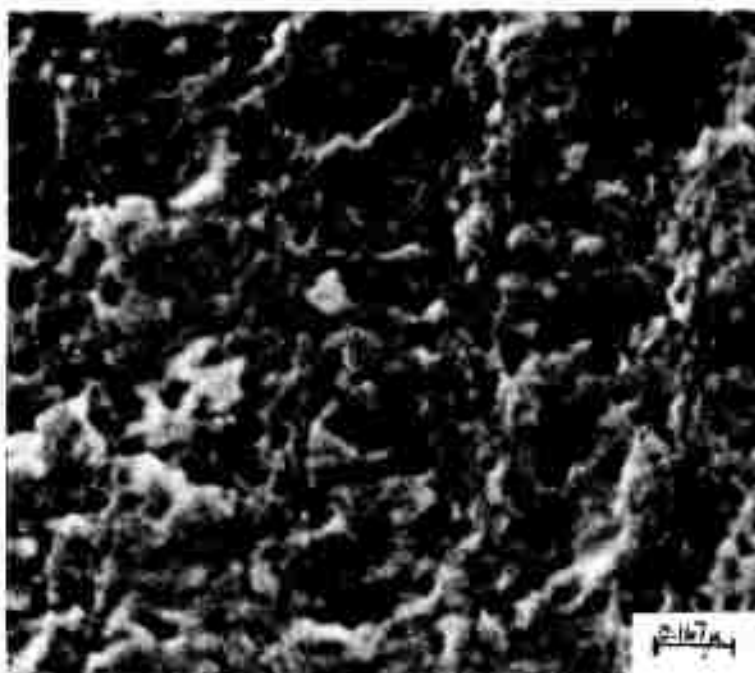
Figure 9.



Sample 317-19, 700°C

10,000X

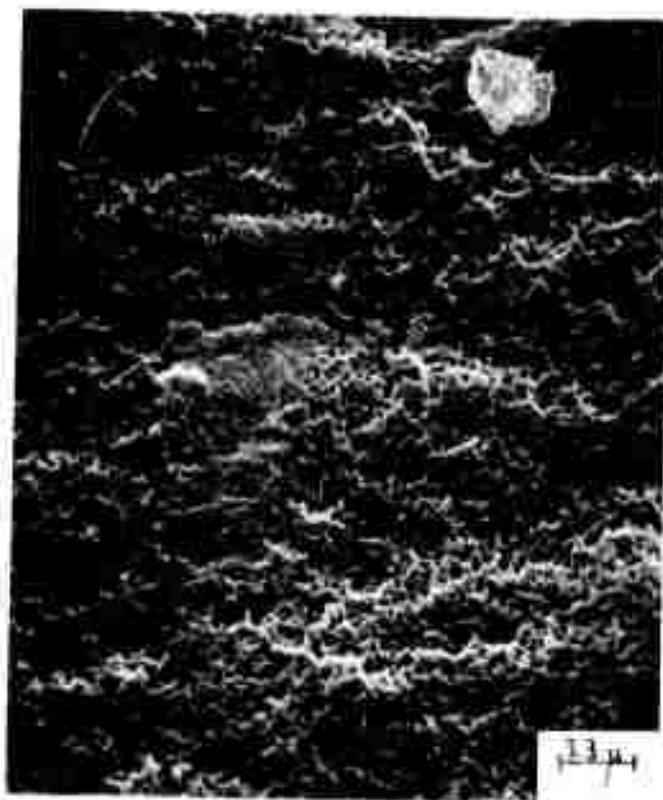
Reproduced from
best available copy.



Sample 317-19, 700°C

60,000X

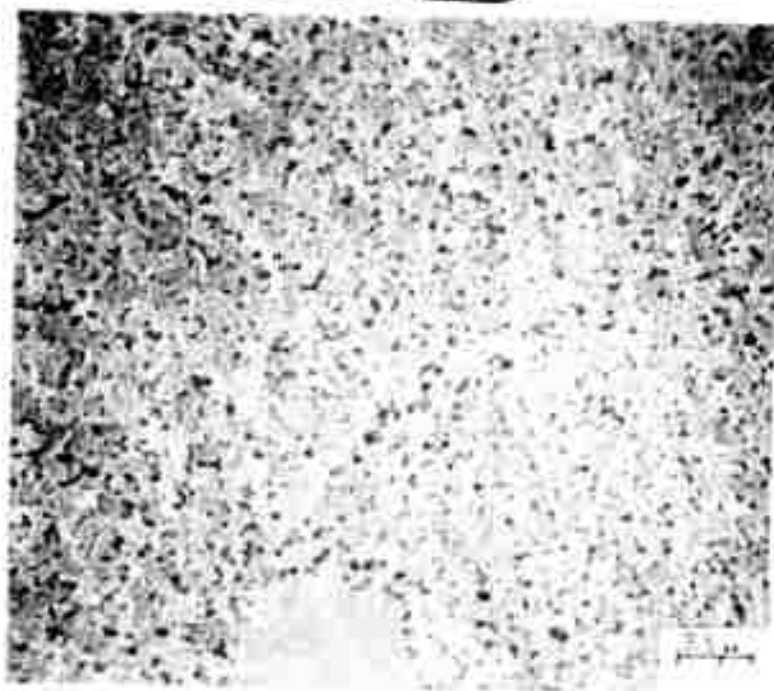
Figure 10.



Sample 321-18, 700°C

3000X

Reproduced from
best available copy.



Sample 321-15, 700°C

3000X

Figure 11.

pycnometer made by Micrometrics Inc. Corporation of Norcross, Georgia. For porous samples, data have been gathered in gross form as well as on 200 mesh powder. Data for samples thus far measured is included in Table 7. Efforts are being made to produce a wide variation in density as well as efforts to improve the accuracy of the measurements.

In addition to real density, the apparent density of the bulk samples is determined geometrically. Table 7 includes the results obtained to date.

Surface Area

No additional surface area data have been gathered since those in Table 5 reported previously¹. However, nitrogen absorption surface areas will be run on the 700°C samples selected after evaluation with Hg porosimetry and scanning electron microscopy.

Mercury Porosimetry

Mercury porosimetry was used to determine pore size distribution, interconnected pore volume, density and median pore diameter values. Data obtained to date are shown in Table 6. Cumulative pore volume-pore diameter curves are shown in Figure 12 for two typical samples. In most cases a rather sharp pore size distribution was observed. In the samples studied the pore sizes ranged over four orders of magnitude from 100 μ to .005 μ depending on the processing variables. A range of total pore volume of a factor of 200 is also shown in Table 6.

The type of distribution indicated in Figure 12 was

TABLE 5

<u>Sample</u>	<u>He Density</u> <u>gm/cm³</u>	<u>Surface Area</u> <u>Knudsen Flow</u> <u>(m²/gm)</u>	<u>Specific Surface</u> <u>Area</u> <u>(m²/gm)</u>
311-32, 2000°C	1.41	3.0	26.4
317-9, 700°C	1.83		506.0
319-9, 2000°C	1.70	12.5	59.9
317-12, 700°C	1.80	9.1	510.0
317-12, 2000°C	1.72		109.0
318-22, 700°C	1.79		459.0
318-22, 2000°C	1.51		49.6

TABLE 6

Sample #	$\rho_{\text{He real}}^1$ (g/cc)	$\rho_{\text{Hg real}}^2$ (g/cc)	$\rho_{\text{Hg app.}}^3$ (g/cc)	MPD ⁴ (μ)	IPV ⁵ (cc/g)
302-5, 4200°F*	--	1.509	.647	2.97	.8828
-12, 4200°F*	--	1.501	.559	3.62	1.1224
305-6, 2000°C*, 6.62 Mo	1.94	1.802	.636	2.54	1.0151
-12, 2000°C*	1.55	1.562	.557	4.19	1.1560
-18, 2000°C*, .4 Mo	1.77	1.718	.606	2.49	1.0678
310-1, 1000°C	1.27	1.446	.814	.023	.5411
-3, 1000°C	--	1.424	.805	.020	.5454
-17A, 2000°C	1.50	1.175	.639	.119	.7130
-18, 1000°C	1.48	1.452	.687	.039	.7666
-18, 2000°C	1.15	1.366	.648	.044	.8110
-20, 2000°C	1.09	1.458	1.029	.009	.2855
-29, 2000°C	1.89	1.533	.944	.014	.3959
311-21, 2000°C	1.59	1.339	.731	.038	.6221
-22, 2000°C	1.00	.847	.484	.154	.8809
312-19A, 730°C	1.20	1.481	.879	.629	.4626
-29, 728°C	1.52	1.441	1.038	.014	.2709
-31, 2000°C	1.41	1.490	.923	.025	.4118
-45, 2000°C	1.26	1.302	1.214	.005	.0540
-48, 2000°C	1.53	1.392	.861	.121	.4425
-49, 2000°C	1.34	1.404	1.031	.011	.2579
315-1, 2000°C	1.50	1.431	.962	47.0	.3412
317-5, 2000°C	1.42	1.313	.873	.071	.4039
-18, 2000°C	1.50	1.255	.953	39.1	.281
318-22, 700°C	1.79	1.426	.771	.057	.5958
-22, 2000°C	1.51	1.576	.937	.054	.4334
308P-2, #2	1.586	1.505	1.034	.009	.3030
-3, #3	1.611	1.486	1.077	.008	.2559
GC No. 1**	1.47	1.482	1.424	.003	.0273

*15,000 psi maximum intrusion pressure; all others 60,000 psi maximum

**Glassy Carbon No. 1 - Le Carbone, p. 6927.

¹Real density as determined by He pycnometry

²Real density as determined by Hg intrusion to 60,000 psi

³Apparent density as determined by Hg

⁴Median pore diameter from Hg porosimetry

⁵Intrusion pore volume from Hg porosimetry

TABLE 7

PHYSICAL PROPERTIES
2000°C Pyrolysis Temperature
(unless otherwise indicated)

Sample #	$\rho_{app.}$ (g/cc)	ρ_{He} (g/cc)	Resistivity ($\Omega\text{-cm} \times 10^{-2}$)	Hardness (DPH)	Internal Friction ($\times 10^{-3}$)	Sonic Mod. psi ($\times 10^6$)	Compressive Strength psi ($\times 10^3$)	Ultimate Strength psi ($\times 10^3$)
311-35	0.51	--	2.94	--	1.43	0.46	--	--
312-33	--	--	--	90	--	--	--	--
312-44	--	--	--	98	--	--	--	--
312-45 (680°C)	--	--	--	135	--	--	--	--
312-45A	--	--	--	176	--	--	--	--
312-46	--	--	--	107	--	--	--	--
312-46 (680°C)	--	--	--	105	--	--	--	--
315-2	0.70	1.50	3.49	--	--	--	--	--
315-20A	0.84	1.59	1.80	--	--	1.69	--	--
315-20B	0.77	1.60	2.75	--	0.93	1.97	--	--
315-29C	0.88	1.60	2.03	--	1.63	1.82	--	--
315-21C	0.91	1.52	1.47	--	0.54	2.03	--	--
315-25C	0.88	1.41	3.17	--	0.26	2.42	--	--
315-26D	0.83	1.45	1.49	--	2.38	2.06	--	--
315-26C	0.80	1.70	0.57	--	--	1.78	--	--
315-31B	0.80	1.62	1.19	--	--	1.60	--	--
315-31C	0.93	1.48	2.37	--	0.33	1.92	--	--
315-31D	0.91	1.46	2.29	--	0.47	2.20	--	--
315-33	0.78	1.50	1.95	--	0.42	2.13	--	--
315-34C	0.60	1.64	2.94	--	1.50	1.68	--	--
315-34D	0.66	1.57	1.37	--	0.31	1.16	--	--
315-37	0.53	1.63	2.62	--	2.01	1.63	--	--
315-38A	0.72	1.71	2.37	--	0.31	2.15	--	--
315-39A	0.96	2.40	1.88	--	--	1.24	--	--
315-39B	0.96	1.64	0.29	--	0.47	2.37	--	--
315-41	0.68	1.67	2.20	--	1.28	2.35	--	--
315-41A	0.77	1.67	0.38	--	--	--	--	--
					1.18	1.80	--	--

Sample #	$\rho_{app.}$ (g/cc)	ρ_{He} (g/cc)	Resistivity ($\Omega\text{-cm} \times 10^{-2}$)	Hardness (DPH)	Internal Friction ($\times 10^{-3}$)	Sonic Mod. psi ($\times 10^6$)	Compressive Strength psi ($\times 10^3$)	Ultimate Strength psi ($\times 10^3$)
315-41B	0.79	1.67	1.57	--	0.98	1.70	--	--
315-42	0.87	1.83	2.49	--	0.35	2.20	--	--
315-44	0.76	1.79	2.14	--	0.32	1.90	--	--
315-45B	0.76	1.39	0.39	--	0.28	7.35	--	--
315-46	--	--	--	240	--	--	--	--
315-46	--	--	--	105	--	--	--	--
315-46A	--	--	--	58	--	--	--	--
317-2	0.71	1.55	--	--	--	--	--	--
317-5	0.78	1.65	0.88	--	--	1.21	23.7	--
317-8	0.90	1.42	--	58	--	--	33.1	7.50
317-10	0.79	1.50	--	--	--	--	40.5	2.29
317-18	0.72	1.42	0.09	--	0.75	1.93	--	--
317-18	0.72	1.50	0.88	--	0.39	1.14	5.1	3.30
317-23	0.83	--	--	--	--	--	7.6	1.90
317-24	0.76	1.57	1.87	--	0.76	1.93	--	--
317-26	0.78	1.27	1.95	14	0.66	2.01	--	--
317-29	0.74	1.46	1.22	--	--	1.14	16.4	2.48
317-32	0.89	1.72	2.24	--	--	2.19	--	3.64
317-33	1.02	--	--	73	--	--	40.2	5.60
317-34	0.65	1.56	3.21	--	--	2.76	--	--
317-37	0.90	1.34	2.25	80	0.31	2.15	40.6	6.90
317-38	0.92	1.72	2.68	62	1.27	1.35	37.6	4.20
317-39	0.77	1.27	0.32	49	0.19	1.60	30.7	5.50
317-40	0.86	1.47	1.84	--	--	1.66	27.1	4.50
317-41	0.93	--	--	--	--	--	10.0	2.35
317-41A	0.90	1.48	--	--	--	--	7.4	1.91
317-41B	1.12	--	--	--	--	--	27.0	3.90
317-42	0.87	1.45	1.35	53	--	2.05	39.8	5.30
317-43	0.90	--	--	--	--	--	15.0	2.47
317-44	0.84	1.51	0.07	52	1.68	1.80	33.3	5.1
317-45	0.88	1.40	--	--	--	--	32.3	5.2
317-46	0.81	1.48	1.12	71	--	1.69	34.6	6.3
317-47	0.97	1.39	--	49	--	--	27.5	--
317-48	1.16	1.46	--	--	--	1.66	--	--
317-49	0.80	1.51	1.67	--	1.31	1.18	--	--

Sample #	$\rho_{app.}$ (g/cc)	ρ_{He} (g/cc)	Resistivity ($\Omega\text{-cm} \times 10^{-2}$)	Hardness (DPH)	Internal Friction ($\times 10^{-3}$)	Sonic Mod. psi ($\times 10^6$)	Compressive Strength psi ($\times 10^3$)	Ultimate Strength psi ($\times 10^3$)
318-1	0.79	1.51	1.69	--	--	0.94	--	2.56
318-7	0.78	1.49	1.65	--	--	0.87	7.1	1.67
318-8	0.96	1.49	--	60	--	--	--	--
318-9	0.96	1.50	--	56	--	--	--	--
318-11	0.91	1.58	--	51	--	1.98	--	5.09
318-12	0.98	1.50	--	61	--	--	--	--
318-13	1.03	--	--	71	--	--	--	--
318-14	0.77	1.47	2.85	31	0.41	0.54	--	--
318-15	0.95	1.48	--	40	--	--	--	--
318-16	0.94	1.49	--	47	--	1.91	28.2	4.02
318-17	0.74	1.48	1.89	53	0.18	1.57	--	4.35
318-18	--	1.46	--	46	--	--	--	--
318-20	--	1.47	--	65	--	--	--	--
318-21	--	1.37	--	56	--	--	--	--
318-22	0.83	1.51	2.37	44	--	1.72	28.0	4.42
318-22	--	--	--	39	--	--	--	--
(700°C)								
318-23	0.91	1.46	--	54	--	--	--	--
318-24	0.97	1.29	--	61	--	1.98	--	--
318-24C	0.96	--	--	--	--	--	25.0	4.47
318-26	0.98	1.54	--	70	--	--	--	--
318-28	0.84	1.45	1.74	--	--	1.77	--	--
318-29	0.63	1.45	1.94	26	--	--	--	--
318-30	1.08	1.49	--	60	--	2.03	--	3.06
318-31	0.55	1.31	2.16	21	2.41	0.18	1.6	0.19
318-32	0.84	--	--	53	--	--	19.7	--
318-33	0.80	1.64	1.01	57	0.73	1.82	--	--
318-34	1.09	1.57	--	--	--	--	28.7	4.85
318-35	0.88	1.40	1.18	--	--	1.98	26.4*	4.57
318-36	0.90	1.43	1.07	67	--	1.80	18.6*	3.34
318-37	0.92	1.48	1.12	--	--	2.90	25.7*	3.90
318-39	1.24	1.50	0.85	--	--	3.99	34.9*	7.95
318-43	1.08	1.51	--	106	--	--	--	--
318-44	1.09	1.51	--	103	--	--	--	--

Sample #	$\rho_{app.}$ (g/cc)	ρ_{He} (g/cc)	Resistivity ($\Omega\text{-cm} \times 10^{-2}$)	Hardness (DPH)	Internal Friction ($\times 10^{-3}$)	Sonic Mod. psi ($\times 10^6$)	Compressive Strength psi ($\times 10^3$)	Ultimate Strength psi ($\times 10^3$)
318-45	1.27	1.52	0.39	--	--	4.12	--	--
318-46	1.02	1.53	0.41	56	--	2.60	42.3*	7.35
318-48	1.04	1.43	--	--	--	--	3.5	8.27
318-50	--	1.49	--	--	--	--	--	5.73
318-51	0.88	1.43	--	--	--	1.10	17.3	1.44
318-52	1.01	1.41	1.30	--	--	2.24	--	--
318-58	0.98	1.36	2.37	--	--	0.13	--	--
318-59	1.18	1.38	--	--	--	--	--	6.02
318-60	0.95	1.71	1.50	54	--	--	31.7	4.20
318-61	1.01	1.75	4.03	--	--	1.96	36.2*	7.63
318-62	0.96	1.39	--	69	--	--	22.6*	3.96
321-3	0.95	1.26	3.40	78	--	--	41.4	6.98
321-6	1.09	1.60	0.31	81	--	--	40.0*	7.18
321-8	0.90	1.38	5.46	105	--	3.11	41.7*	8.27
321-9	1.17	1.46	--	120	--	1.97	38.9*	7.00
321-10	1.26	1.43	1.00	99	--	--	54.2	9.75
321-11	0.95	1.46	1.14	95	--	3.99	54.9*	10.85
321-11C	--	--	--	132	--	2.05	32.3	5.81
321-12	0.97	1.46	1.21	--	--	--	--	--
321-13	0.95	1.46	1.15	131	--	1.63	13.9	2.52
321-15	0.96	1.43	--	--	--	2.22	36.2	6.04
321-16A	0.85	--	--	--	--	--	34.5	5.98
321-17B	0.94	--	--	--	--	--	24.3	4.47
321-18B	0.64	--	--	--	--	--	36.7	5.26
321-19A	0.87	--	--	115	--	--	39.6	5.85
321-19B	0.83	--	--	87	--	--	31.5	6.84
							31.4	5.76

*head speed .05 in/min, all others .02 in/min.

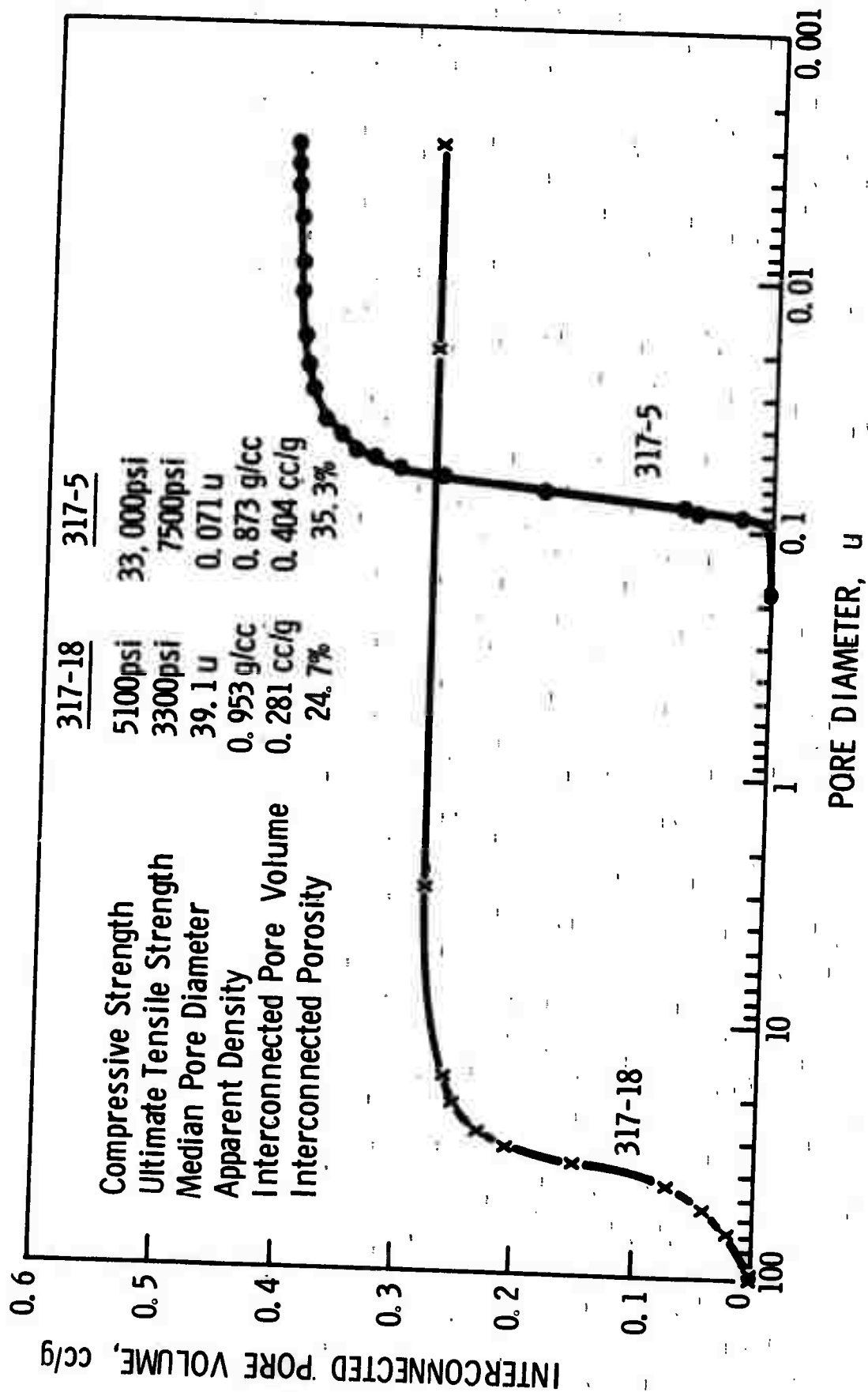


Figure 12

observed in most of the samples studied, however, in several samples an increase in penetration was observed at the upper limit of the 60,000 psi porosimeter as shown in Figure 13. This would tend to indicate that pores smaller than 30\AA were present. Depressurization curves are also shown in Figure 13. An interesting observation was that the intruded mercury did not come out of the sample until the pressure was reduced to below 14.7 psi (pore size $>100\mu$). The nature of this observation is not clearly understood and warrants further investigation. In addition, these particular samples must be studied further to determine if open pores smaller than 30\AA exist or if the increase in mercury penetration is due to failure of the material (collapsing of closed voids) at the higher intrusion pressures.

IV. Property Evaluation

Because the glassy carbons under investigation were produced under a wide range of processing variables, a large degree of variation in structure and physical properties was observed. Based on previous information some of which was included in a previous report¹, several tests were chosen as a means of obtaining preliminary mechanical property data. The mechanical properties investigated thus far include hardness (DPH), compressive strength, ultimate tensile strength (Diametral compression) and sonic modulus of elasticity. In addition, internal friction and electrical resistivity were measured on selected samples.

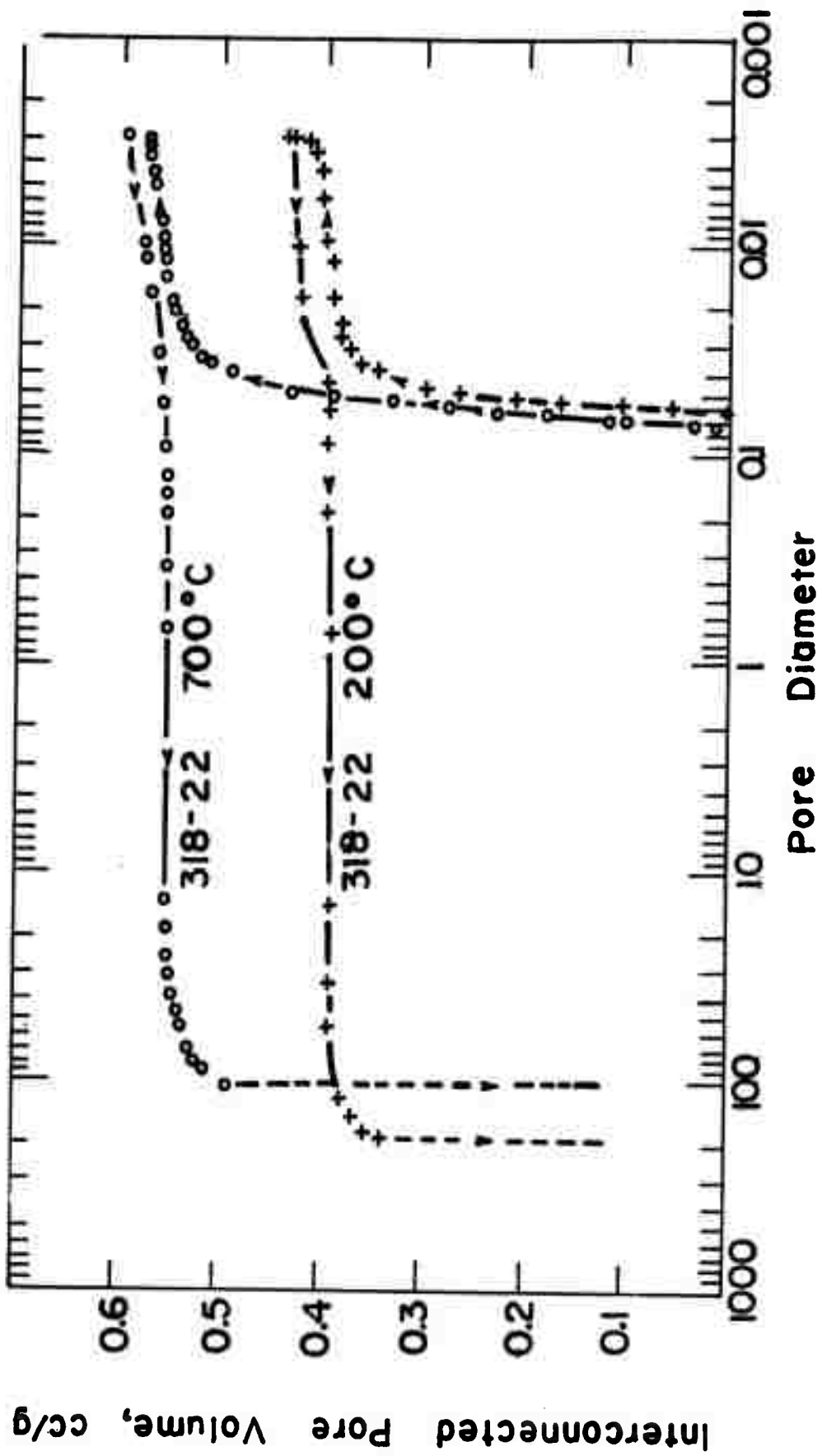


Figure 13

Hardness

Diamond Pyramid (DPH) values were obtained with a Tukon* hardness tester utilizing a standard load cycle. For most of the experimental carbons previously tested¹ it was observed that with loads greater than 3Kg little or no substantial increase in hardness was obtained and extensive cracking or crushing occurred in many cases. In addition, a weird recovery phenomena was observed and in some cases a hardness indentation was observed only if a thin collodion film was applied to the surface of the test sample prior to conducting the test.

Based on this prior information a routine procedure was established for screening the available glassy carbon materials and new carbon materials as they are produced. Hardness determinations were made on each material with and without a collodion film present and also at two loads, 1 kilogram and 3 kilograms.

Hardness data obtained in this manner is shown in Table 7. Hardness values for the commercially available glassy carbons were slightly higher when no coating was applied and little variation in hardness was noted as a function of load. Similar results were noted for the experimental carbons with an exception occurring for the 321 series of samples produced at 1000°C. Samples in this series tested at 3Kg exhibited higher hardness values than those tested at a load of 1Kg.

*Wilson Mechanical Instrument Div., American Chain & Cable Co., Inc., New York, N.Y.

Satisfactory indentations were obtained in approximately 2/3 of the samples tested. Because of variations in pore structure or variations in an elastic behavior unreadable impressions were obtained in the remainder of the samples. The indentations in these samples appeared under the measuring microscope as a blur or an "x". The majority of the values obtained were much lower than was expected, however the information is useful in that relative hardness values and information concerning the elastic recovery behavior of the carbons under investigation was obtained. Development of test methodology for obtaining hardness values more consistent with the scratch hardness displayed by the material is currently in progress.

The range of hardness values reported for both the commercial samples and the experimental samples is not consistent with the scratch hardness of the material. All of these materials easily scratch glass, which should place this hardness in excess of 800 VHN. However, even the hardest of the group give readings of 300 or below. Since these materials have a relatively low modulus, it is possible that the impressions being measured are traces of the impression existing under load and not the residual impression. In order to check this postulate, a sample was loaded to 3Kg and then examined with a scanning electron microscope where the depth of field qualities can more easily bring out the residual impression. Figure 14 shows the results on one uncoated sample. A large marking is visible surrounding the smaller residual impression. Cracks are clearly visible that could not



Figure 14. Scanning micrograph (500X) of 321-9, 2000°C after 3KG Vickers Indentation. Note Large Area of Impression Outside the Smaller Unrecovered Inner Impression.

be seen in the optical microscope. The large impression which must have existed under load corresponds to a VHN of 170, which compares reasonably well with the regular determination of 120 given in Table 7. However, the true impression gives a much higher hardness of about 3400 VHN. This value seems too high and may be in error due to the fracturing that occurred. Additional data at lower loads will be run to confirm this effect. However, it is certain that most of the measurements to date have not truly reflected the hardness. Depth of penetration hardness tests also will yield anomalous results in materials like these due to the very low modulus ($4 \cdot 10^6$ psi) compared with the high strength.

Compressive and Ultimate Tensile Strength

A feasibility study is currently in progress to determine the most satisfactory method for producing compressive strength and ultimate tensile strength test samples. To date samples have been produced by the following methods:

- machining glassy carbon stock prior to pyrolysis
- machining glassy carbon stock
- core drilling glassy carbon stock
- centerless grinding
- hand lapping
- machine lapping

Preliminary evaluation of these methods indicates that the most feasible method of sample preparation is by centerless grinding and lapping for flatness.

Preliminary strength data obtained from samples produced by the various methods mentioned above are shown in Table 7. The majority of the tensile strength samples were 3/8" in diameter and 3/4" long. The diametral compression test was used to obtain ultimate tensile strength data. Samples for the diametral compression test were 3/8" by 3/32" long.

Most samples were tested in an Instron testing machine with a cross-head speed of .02"/min. Blotter paper pads were used as cushions between the machine platen and the test piece in both the compressive and diametral tests.

The compressive strength data included in this report ranged up to 54,900 psi, while ultimate tensile strength data ranged up to 10,850 psi. Data reported represents at least two samples. In most cases four to six samples will be included although not all samples have been tested at present.

In Table 8 the data have been correlated with apparent and helium density. Since the fraction of the sample occupied by carbon is $\rho_{\text{apparent}}/\rho_{\text{He}}$, an additional correlation has been presented in Table 8 reflecting the strength properties relative to the carbon present. The specific properties show a narrower range, but are by no means constant for all of the carbons.

Sonic Modulus and Internal Friction

The sonic modulus of elasticity and the internal friction of glassy carbons are both determined using the Michigan Intermediate Frequency Electrostatic Resonator (MIFER). The samples used are cylindrical rods about 3/8" in diameter and 5" long.

TABLE 8

PHYSICAL PROPERTIES CORRELATED WITH DENSITY
(2000°C Pyrolysis Temperature)

Sample #	$E_s/\rho_{app.}$ (in $\times 10^6$)	$\sigma_{cs}/\rho_{app.}$ (in $\times 10^3$)	$\sigma_{UTS}/\rho_{app.}$ (in $\times 10^3$)	$E_s \left(\frac{\rho_{He}}{\rho_{app.}} \right)$ (psi $\times 10^6$)	$\sigma_{cs} \left(\frac{\rho_{He}}{\rho_{app.}} \right)$ (psi $\times 10^3$)	$\sigma_{UTS} \left(\frac{\rho_{He}}{\rho_{app.}} \right)$ (psi $\times 10^3$)
315-2	67.1	--	--	3.62	--	--
-20A	65.1	--	--	3.73	--	--
-20B	65.7	--	--	3.78	--	--
-20C	64.1	--	--	3.69	--	--
-21C	73.9	--	--	4.04	--	--
-25C	65.0	--	--	3.30	--	--
-26D	59.6	--	--	3.10	--	--
-26C	55.6	--	--	3.40	--	--
-31B	66.7	--	--	3.89	--	--
-31C	65.7	--	--	3.50	--	--
-31D	65.0	--	--	3.41	--	--
-33	59.8	--	--	3.23	--	--
-34C	53.7	--	--	3.17	--	--
-34D	68.6	--	--	3.88	--	--
-37	112.7	--	--	6.61	--	--
-38A	47.8	--	--	2.95	--	--
-39A	68.6	--	--	5.93	--	--
-39B	68.0	--	--	4.01	--	--
-41A	64.9	--	--	3.90	--	--
-41B	61.3	--	--	3.59	--	--
-42	70.2	--	--	4.63	--	--
-44	69.4	--	--	4.48	--	--
-45B	268.6	--	--	13.44	--	--
31-2	47.3	922	--	2.81	55.1	--
-5	--	1175	266	--	56.1	13.7
-8	--	1247	70.5	--	67.5	3.8
-10	67.9	--	--	3.47	--	--
-18	44.0	126	104	2.38	10.6	6.9
-23	--	254	63.4	--	--	--
-24	70.5	--	--	3.99	--	--
-26	71.6	--	--	3.27	--	--

Sample #	$E_s/\rho_{app.}$ ($\text{in} \times 10^6$)	$\sigma_{cs}/\rho_{app.}$ ($\text{in} \times 10^3$)	$\sigma_{UTS}/\rho_{app.}$ ($\text{in} \times 10^3$)	$E_s \left[\frac{\rho_{He}}{\rho_{app.}} \right]$ ($\text{psi} \times 10^6$)	$\sigma_{cs} \left[\frac{\rho_{He}}{\rho_{app.}} \right]$ ($\text{psi} \times 10^3$)	$\sigma_{UTS} \left[\frac{\rho_{He}}{\rho_{app.}} \right]$ ($\text{psi} \times 10^3$)
-29	42.8	615	92.8	2.24	32.4	4.9
-32	68.4	--	113	4.23	--	7.0
-33	--	1092	152	--	57.5	--
-34	117.9	--	--	6.62	--	--
-37	66.4	1049	212	3.20	60.4	10.3
-38	41.7	1158	126	2.58	71.9	7.9
-39	57.7	1105	198	2.64	50.6	9.1
-40	54.2	884	145	2.87	46.9	7.7
-41	--	298	70.0	--	--	--
-41A	--	228	58.8	--	--	--
-41B	--	668	96.5	--	35.8	--
-42	65.5	1266	169	3.50	66.3	8.8
-43	--	462	76.0	--	23.4	--
-44	59.5	1097	168	3.24	59.9	9.2
-45	--	1017	164	--	51.4	--
-46	58.0	1183	215	3.09	63.2	9.7
-47	--	785	131	--	39.3	--
-48	39.8	--	--	2.09	--	--
-49	41.0	--	--	2.23	--	--
318-1	33.1	--	89.8	1.80	--	4.9
-7	30.9	252	28.0	1.66	13.6	3.2
-11	60.4	--	155	3.44	--	8.8
-14	19.5	--	--	1.01	--	--
-16	56.4	831	118	3.01	44.4	--
-17	58.9	--	163	3.10	--	8.7
-22	57.6	933	148	3.07	49.9	--
-24	56.7	--	--	2.63	--	--
-24C	--	715	129	--	33.3	--
-28	58.5	--	--	3.06	--	--
-30	52.2	--	78.5	2.80	--	4.2
-31	9.1	80.3	9.6	0.43	3.8	0.5
-32	--	650	--	--	37.1	--
-33	62.5	--	--	3.69	--	--
-34	--	729	123	--	38.1	--
-35	62.5	831	144	3.15	42.0	7.3

Sample #	$E_s/\rho_{app.}$ (in $\times 10^4$)	$c_{cs}/\rho_{app.}$ (in $\times 10^3$)	$c_{UTS}/\rho_{app.}$ (in $\times 10^3$)	$E_s \left(\frac{\rho_{He}}{\rho_{app.}} \right)$ (psi $\times 10^3$)	$c_{cs} \left(\frac{\rho_{He}}{\rho_{app.}} \right)$ (psi $\times 10^3$)	$c_{UTS} \left(\frac{\rho_{He}}{\rho_{app.}} \right)$ (psi $\times 10^3$)
318-36	56.8	573	103	2.86	29.6	5.3
-37	87.6	773	117	4.67	41.3	6.3
-39	89.4	778	178	4.83	42.2	9.6
-45	90.1	--	--	4.93	--	--
-46	70.8	1149	200	3.90	63.5	11.0
-48	--	93.2	220	--	4.9	--
-50	--	--	--	--	--	--
-51	34.7	546	45.3	5.64	28.2	2.3
-52	61.6	--	--	3.13	--	--
-58	3.7	--	--	0.18	--	--
-59	--	--	165	--	--	8.4
-60	--	744	98.6	--	39.8	--
-61	53.9	1055	222	--	65.2	13.7
-62	--	620	109	3.40	39.2	6.9
321-3	--	1195	201	--	60.2	--
-6	--	1166	209	--	53.1	9.5
-8	79.3	1061	210	4.57	61.3	12.1
-9	60.8	1197	215	3.02	59.6	10.7
-10	--	1283	231	--	63.2	--
-11	88.0	1207	238	4.53	62.3	12.3
-12	59.9	942	169	3.15	49.6	8.9
-13	46.7	396	72	2.45	20.9	3.8
-15	64.9	1032	176	3.41	54.5	9.3
-16A	--	994	173	--	51.4	8.9
-17B	--	792	146	--	--	--
-18B	--	1089	155	--	--	--
-19A	--	1726	254	--	--	--
-19B	--	1006	218	--	--	--
	--	1055	192	--	--	--

These rods are set into longitudinal vibration by electrostatic forces from an electrode positioned within 0.001" from the sample. The surfaces of the rod and electrode must be parallel in order to get sufficient amplitude to distinguish the resonant frequency of the sample.

The resonant frequency is determined by changing the exciting frequency by an oscillator until the maximum amplitude signal is displayed on an oscilloscope. There is generally a large increase in the signal amplitude when resonance is reached. Once the resonant frequency has been determined, the sonic modulus can be calculated using the following formula,

$$E_s = \frac{L^2 \rho f_n^2}{72}$$

where L is the length of the rod in inches, ρ is the apparent density in lb/in³, and f_n is the resonant frequency in cps.

The internal friction is determined by measuring the half-amplitude decay time of the resonant signal on the oscilloscope. This is accomplished by turning off the exciting frequency and photographing the exponential decay pattern on the oscilloscope. Knowing the scale of the sweep, the half-amplitude decay can be easily determined. The internal friction is then calculated using the following formula,

$$Q^{-1} = \frac{\ln 2}{\pi f_n t^{\frac{1}{2}}}$$

where f_n is the resonant frequency and $t^{\frac{1}{2}}$ is the half-amplitude decay time. Some examples of decay patterns of glassy carbons

and aluminum are shown in Figures 15 and 16.

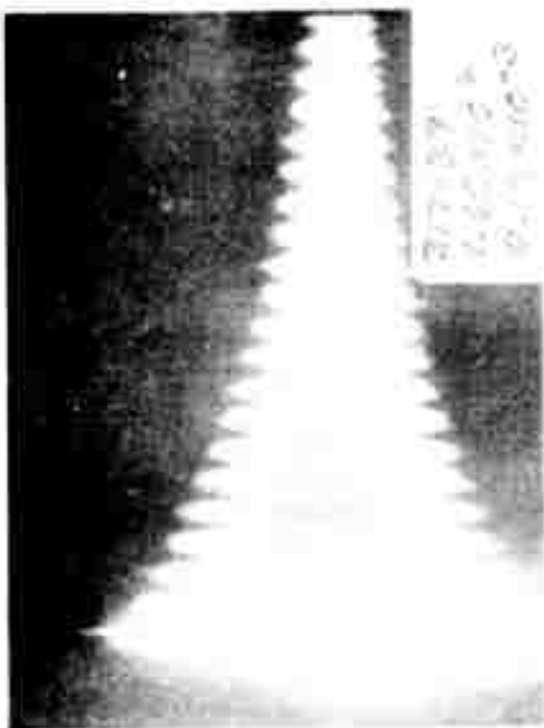
Through examination of Table 7, it can be seen that the sonic modulus varies from 0.18×10^6 to 7.35×10^6 psi and the internal friction varies from 0.19×10^{-3} to 2.38×10^{-3} for 2000°C samples. The shape of the decay patterns (Figures 15 and 16) varies considerably from sample to sample. This may possibly be caused by pore size effects, which cause the rippled pattern. Generally, it has been observed that coarser pored samples give more pronounced ripples in the pattern. A sample of aluminum has been included in Figure 16 for comparison purposes.

Further study has been done to establish the effect of pyrolysis temperature on the sonic modulus. This data is shown in Table 9. The general trend of the data shows the maximum modulus to result from pyrolysis between 1000°C and 1577°C. More samples must be studied to narrow this gap further. In all cases the cured, but unpyrolyzed samples show an order of magnitude lower modulus. It has not yet been possible to measure the internal friction in the as-cured condition.

Electrical Resistivity

The resistivity of glassy carbons heat treated to 800°C or higher, is very low. Therefore a special type of set-up is required in order to get accurate determination of the resistance. In this case, a brass cylinder with steel wool pads was used to eliminate surface affects. This set-up when used with the proper ohm-meter allows accurate determination down to 0.01 ohm.

The resistivity is determined by the formula,



Reproduced from
best available copy.

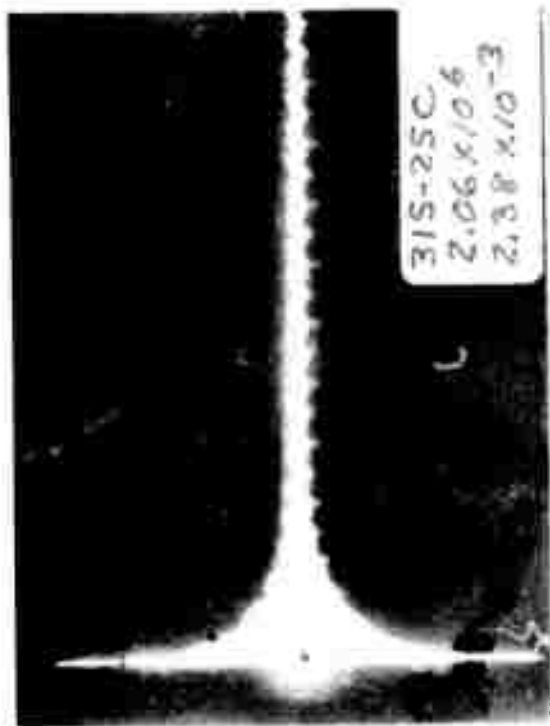
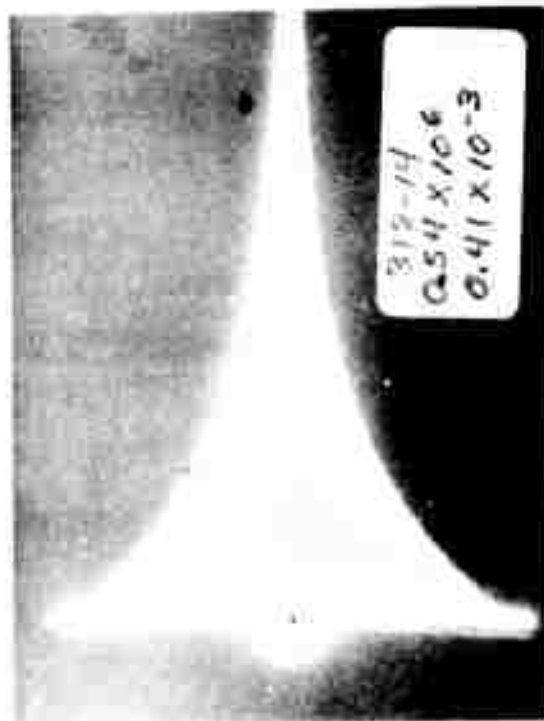
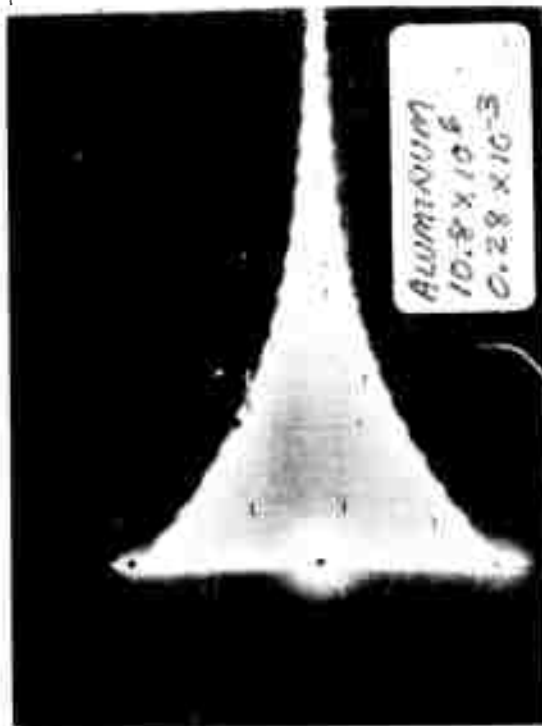
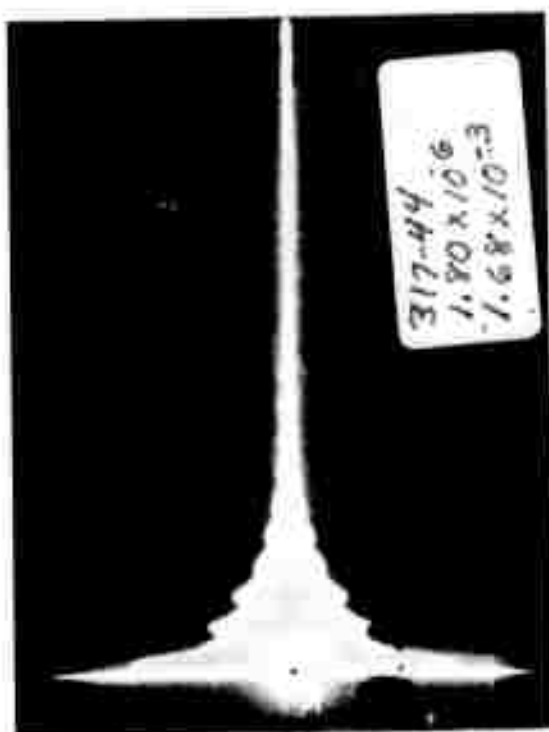


Figure 15. Decay patterns from glassy carbon samples. Top number is sample number, then modulus, then internal friction.



Reproduced from
 best available copy.

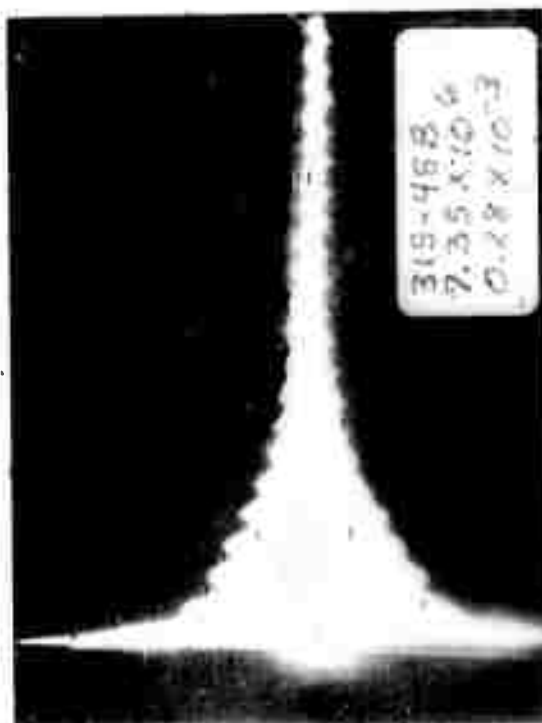
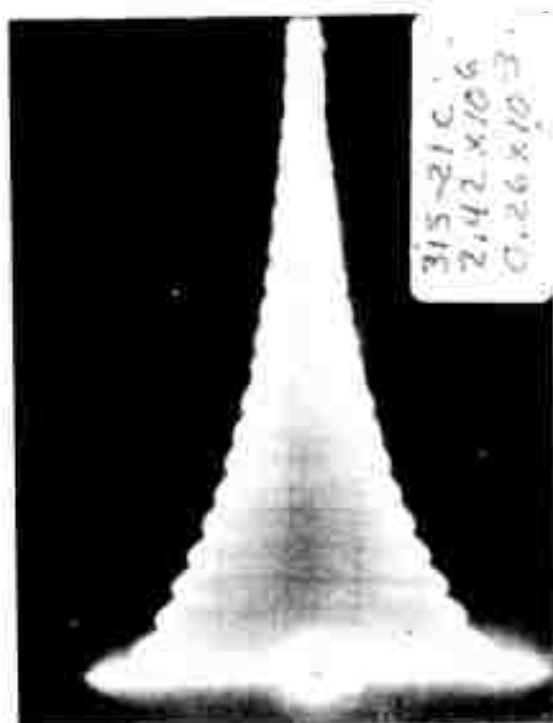


Figure 16. Decay patterns from three glassy carbon samples and one aluminum rod.

TABLE 9

PYROLYSIS
SONIC MODULUS (psi $\times 10^6$) vs. TEMPERATURE ($^{\circ}\text{C}$)

Sample #	700 $^{\circ}\text{C}$	800 $^{\circ}\text{C}$	900 $^{\circ}\text{C}$	1000 $^{\circ}\text{C}$	1577 $^{\circ}\text{C}$	1800 $^{\circ}\text{C}$	2000 $^{\circ}\text{C}$
321-11L	1.00			2.37	2.24	2.29	2.11
321-11CL	0.98			2.34	2.33	2.29	2.21
321-12L	0.89			1.96	2.10	1.64	1.57
321-13 #1L	1.07			2.46	2.36	2.31	2.33
321-13 #2L	1.10			2.47		2.38	2.29
321-13 #3L	1.17			2.55		2.33	2.29
318-59 #1L	1.47			2.88	2.60	2.36	1.95
318-59 #2L	1.41			2.76	2.80	2.42	2.34
318-60L	1.24				2.43	2.36	2.27
321-15L		2.25		2.75	2.50	2.48	2.38
321-16AL		2.09		2.62	2.49	2.22	2.11
321-18BL		2.08		2.13	2.53	2.44	2.33
321-19BL		1.87		2.87	2.17	2.19	2.06
321-17B	0.80		2.41	2.84	2.61	2.55	2.41
321-15 #1	1.08		2.26	2.55	2.54	2.45	2.25
321-19B #1	1.00		4.78	2.11	1.57	1.99	1.99
321-16B		2.24		2.50	2.24	2.07	1.97
321-15 #2		2.04		2.62	2.68	2.48	2.28
321-18B #1		2.31		2.64	2.48	2.41	2.31
321-16A		2.14		2.51	2.49	2.26	2.06
321-19A		2.05		2.71	2.61	2.52	2.44
321-18A		2.17		2.94	2.85	2.78	2.64
321-19B #2		1.76		2.25	2.15	2.15	2.06
321-18B #2		2.04		2.63	2.78	2.32	2.31

$$\rho = \frac{RA}{L}$$

where R is the resistance in ohms, A is the cross sectional area of the sample in cm², and L is the length of the sample in cm. The resistivity of various 2000°C samples is shown in Table 7. It varies from 0.07×10^{-2} to 5.46×10^{-2} Ω-cm.

A study of the affect of temperature on resistivity was also made. The results are shown in Table 10. These data show, as expected, that the resistivity decreases markedly as the heat-treatment temperature increases. This is a general trend, however, there are a few exceptions. The resistivity of the samples in the as-cured state is of course many orders of magnitude larger.

Since geometric data is required for both the modulus and resistivity determinations, apparent density was measured accurately for a series of samples as a function of pyrolysis temperature. These data are shown in Table 11. The apparent density generally decreases slightly with increasing pyrolysis temperature. This is contrary to the usual findings. In this particular series, the same samples were successively heated in vacuum to each higher temperature after holding for about 1 hour, followed by property measurements at room temperature.

TABLE 10

Sample #	PYROLYSIS RESISTIVITY ($\Omega\text{-cm}$) ($\times 10^{-2}$) vs. TEMPERATURE ($^{\circ}\text{C}$)					
	800 $^{\circ}\text{C}$	900 $^{\circ}\text{C}$	1000 $^{\circ}\text{C}$	1577 $^{\circ}\text{C}$	1800 $^{\circ}\text{C}$	2000 $^{\circ}\text{C}$
321-11L			0.643	0.116	0.120	0.120
321-11CL			0.471	0.098	0.090	0.170
321-12L			0.542	0.148	0.120	0.06
321-13 #1L			0.506	0.120	0.170	0.100
321-13 #2L			0.521	0.106	0.160	0.110
321-13 #3L			0.490	0.111	0.110	0.110
318-59 #1L			0.499	0.102	0.080	0.120
318-59 #2L			0.522	0.099	0.080	0.060
318-60L			0.523	0.108	0.160	0.170
321-17B		0.830	0.800	0.357	0.180	0.180
321-15 #1		1.430	0.140	0.302	0.150	0.150
321-19B #1		1.710	0.170	0.368	0.180	0.180
321-16B	4.450		0.300	0.328	0.170	0.170
321-15 #2	4.480		0.290	0.319	0.150	0.150
321-18B #1	6.110		0.590	0.334	0.160	0.160
321-16A	2.790		0.140	0.290	0.150	0.150
321-19A	3.170		0.310	0.332	0.170	0.170
321-18A	2.380		0.280	0.368	0.170	0.170
321-19B #2	3.020		0.300	0.325	0.160	0.160
321-18B #2	3.580		0.180	0.333	0.200	0.190
321-15L	3,240		0.110	0.115	0.170	0.110
321-16AL	3.660		0.170	0.089	0.120	0.100
321-18BL	3.740		0.160	0.114	0.110	0.110
321-19BL	3.550		0.150	0.081	0.110	0.110

TABLE 11

Sample #	PYROLYSIS DENSITY (g/cc) vs. TEMPERATURE (°C)						
	700°C	800°C	900°C	1000°C	1577°C	1800°C	2000°C
321-11L	1.00			0.94	0.93	0.93	0.92
321-11CL	0.99			0.95	0.92	0.92	0.92
321-12L	1.00			0.97	0.91	0.91	0.92
321-13 #1L	0.98			0.97	0.91	0.92	0.94
321-13 #2L	0.98			0.98	0.93	0.92	0.92
321-13 #3L	0.98			0.96	0.90	0.93	0.92
318-59 #1L	1.04			1.06	1.04	1.01	1.01
318-59 #2L	1.03			1.03	1.02	1.01	1.01
318-60L	0.90			0.92	0.92	0.92	0.92
321-17B	0.85		0.96	1.00	0.94	0.94	0.95
321-15 #1	0.88		0.95	0.97	0.94	0.93	0.93
321-19B #1	0.77		0.86	0.88	0.85	0.84	0.85
321-16B		0.93		0.95	0.88	0.87	0.87
321-15 #2		0.91		0.96	0.99	0.93	0.93
321-18B #1		0.89		0.94	0.89	0.90	0.89
321-16A		0.88		0.91	0.88	0.88	0.86
321-19A		0.94		0.97	0.94	0.94	0.94
321-18A		0.95		0.99	0.97	0.96	0.96
321-19B #2		0.88		0.92	0.88	0.89	0.88
321-18B #2		0.89		0.93	1.02	0.87	0.88
321-16AL		0.86		0.93	0.91	0.85	0.85
321-19BL		0.88		0.91	0.86	0.88	0.86
321-18BL		0.90		0.93	0.88	0.90	0.90
321-15L		0.95		0.98	0.92	0.94	0.94

References

1. Glassy Carbons, Semi-Annual Progress Report, January 1972, Contract No. DAHC15-71-C-0283.
2. M. A. Short and P. L. Walker, Carbon 1 (1), 1, 1961.
3. E. E. Hucke and S. K. Das, "A Proposed Method for the Evaluation of the Thermodynamic Properties of the Glassy Carbon-Graphite Equilibrium," Final Report of the Materials Research Council, January 1972, Contract No. DAHC15-71-C-0253.